WMRC Reports
Waste Management and Research Center

Applicability of Microfiltration for Recycling Semi-Synthetic Metalworking Fluids

John E. Wentz
Shiv G. Kapoor
Richard E. DeVor
Department of Mechanical and Industrial Engineering
University of Illinois at Urbana-Champaign

Nandakishore Rajagopalan
Illinois Waste Management and Research Center

Applicability of Microfiltration for Recycling Semi-Synthetic Metalworking Fluids

John E. Wentz
Shiv G. Kapoor
Richard E. DeVor
Department of Mechanical and Industrial Engineering
University of Illinois at Urbana-Champaign

Nandakishore Rajagopalan
Illinois Waste Management and Research Center
Champaign, Illinois

December 2007

TABLE OF CONTENTS

LIST OF TABLES

LIST OF FIGURES

NOMENCLATURE

B – Percent of Tramp Oil Rejected by Membrane

C_p – Tramp Oil Concentration in Permeate

C_r – Tramp Oil Concentration in Feed

CWF – Clean Water Flux

D – Particle Separation Distance

e – Charge on an Electron

F_{dl} – Interparticle Electrostatic Interaction Force

F_E – Electrostatic Interaction Force between Particle and Surface

J – Permeate Mass Flux

k – Boltzmann Constant

K_{PCM} – Rate Constant for Membrane Resistance

LMH – Liters/m^2/hour a measure of flux

MWF – Metalworking Fluid

ΔP – Transmembrane Pressure

Q_0 – Initial Volumetric Permeate Flow Rate

R – Particle Radius

R_{ef} – Resistance Due to External Fouling

R_f – Resistance Due to Fouling

R_{if} – Resistance Due to Internal Fouling

R_m – Intrinsic Membrane Resistance

R_0 – Initial Membrane Resistance

R_t – Total Resistance

SEM – Scanning Electron Microscope

t – Time

T - Temperature

W_{dl} – Interparticle Interaction Energy

z – Number of Charges on an Ion

ε - Dielectric Constant

ε_0 – Permittivity of Free Space

κ - Inverse Debye Length

ν_p – Kinematic Viscosity

ψ_m – Membrane Surface Potential

ψ_p – Particle Surface Potential

EXECUTIVE SUMMARY

The machining industry is heavily dependent on metalworking fluids (MWFs) for both cooling and lubrication. However, the use of these fluids comes at the price of high disposal costs and health risks to workers. Microfiltration has been shown to be a viable method of recycling synthetic MWFs while reducing harmful microbe populations. The extension of this technology has also been shown for a single semi-synthetic MWF. The primary obstacle in the use of microfiltration is the fouling (clogging) of the microfiltration membranes. This research seeks to investigate the applicability of microfiltration technology by investigating the membrane fouling mechanisms at work in the system. It also aims to reduce fouling through adjustment of operating parameters and the design of a new semi-synthetic MWF that significantly reduces the impact of membrane fouling.

Tests to determine the mode and intensity of membrane fouling for three concentrations of an uncontaminated commercial semi-synthetic MWF were conducted at low transmembrane pressure, high cross-flow velocity, with the membrane backpulsed every 2 minutes for 1 second using tubular α-alumina membranes. Steady-state fluxes for the system were recorded in the 200-300 LMH (Liters/m^2/hour) range. It was found that the concentration of the MWF did not have an effect on the steady-state flux reached by the system. A review of the data leads to a two-stage model for membrane fouling that starts with the formation and deposition of micro-emulsion aggregates on the membrane surface followed by the formation of a cake layer that is partially able to be removed by surfactant washings. These mechanisms are driven by hydrodynamic drag forces on

11

particles overcoming repulsive electrostatic forces between particles. When this happens the micro-emulsions create the aggregates that contribute to membrane fouling. This was confirmed by Scanning Electron Microscope (SEM) imaging of fouled membranes.

A 2^3 factorial experiment was carried out on the uncontaminated commercial MWF to determine the effect of operational parameters on membrane fouling. All of the three parameters tested; transmembrane pressure, cross-flow velocity, and backpulsing, were found to be important along with the interaction of pressure and backpulsing. In the presence of a cake fouling layer, it was found that flux is responsive to changes in transmembrane pressure only in the presence of backpulsing and in its absence flux is solely dependent on cross-flow velocity. Backpulsing was also found to be most effective for systems that are run at high pressures. It was determined that the best available parameter settings were high pressure and velocity in the presence of backpulsing. The results of the experiment confirmed the two-stage fouling model mentioned earlier.

The ability of the microfiltration membranes to remove fluid contaminants was tested by the introduction of hydraulic and way oils into the MWF during processing. It was found that the system was able to remove the extraneous oils at rates in excess of 96% while maintaining the same steady-state flux as recorded for the uncontaminated MWF.

The problem of membrane fouling was further addressed through the development of a semi-synthetic MWF specifically designed to reduce membrane fouling. The fluid was

engineered based on understanding the fouling phenomena and using MWF components that maximize the magnitude of the interparticle electrostatic forces that are responsible for reducing membrane fouling. The designed fluid was tested in the microfiltration system and found to maintain a constant flux at a value close to twice that of the commercial semi-synthetic fluid. There was no evidence of the continuous membrane fouling that plagued earlier attempts with the commercial semi-synthetic MWF. In addition the designed fluid was tested on both tapping-torque and drilling testbeds to determine its ability to perform typical MWF tasks of cooling and lubricity. In these tests, the performance of the designed fluid could not be distinguished from that of the commercial MWF in tests of cooling and lubricity.

1. INTRODUCTION

The machining industry is heavily dependent on metalworking fluids (MWFs) for cooling and lubricating of the workpiece and tool, transporting chips from the cutting zone and imparting corrosion resistance to the machined surfaces. While necessary, these fluids cause a large strain on the economy and the environment [1]. They are also a major health concern due to potential health risks associated with bacterial growth during use [2]. MWFs become process effluents that require disposal at significant cost [3] when contaminants such as tramp oils, particulate debris, and bacterial growth attain levels that can adversely affect functionality [4]. Technologies such as conventional cartridge filtration, coalescers, and centrifugation have all been used for recycling of MWFs but are limited in their capability to remove particulate matter that is less than 10 μm in diameter. They also fail to remove tramp oil emulsions and bacterial contamination. Microfiltration is a membrane-based technology that overcomes these issues as well as eliminating the need for biocides with potentially harmful side-effects. However, microfiltration can lose its effectiveness when the pores of the membrane become clogged by the fluid and contaminants [5,6]. This clogging is referred to as membrane fouling and it occurs when components within the MWF or contaminating agents block or constrict the pores of the membrane and cause reduced system flow rate and a lower quality of the filtered MWF.

Most microfiltration studies have focused on synthetic MWFs. This is because microfiltration of a synthetic MWF is a relatively simple separation because the primary ingredients of the fluid are water soluble, while the contaminants are all either colloidal

14

or particulate [5,7,8]. A successful process for recovering synthetic MWF used during the grinding of aluminum was developed by Rajagopalan et al [9]. A membrane-based recycling system for synthetic coolant was developed and field-tested by Mahdi et al. [7,8]. Skerlos et al. [5,6] investigated how the flux of a synthetic MWF was affected by physical obstruction to permeation, also known as membrane fouling, and also studied the impact of microfiltration on microbial growth [10]. Belfort et al. [11] identified three types of membrane fouling: pore constriction, pore blocking, and cake formation.

Although significant microfiltration-based work has been accomplished with synthetic MWF, synthetics only make up 21% of the market. The remainder consists of semi-synthetic (24%) and soluble oil (55%) MWFs [12]. The microfiltration of semi-synthetic MWFs, which constitute a growing market share [1,13], is more difficult as it entails selective separation of contaminants from the native MWF micro-emulsions. Rajagopalan et al. [14] showed for the first time that microfiltration is a technically viable option for purifying a semi-synthetic MWF. However, little is known about how applicable this technology is for semi-synthetic MWFs, primarily due to lack of knowledge about the mechanisms that cause membrane fouling and how to best combat these mechanisms.

The goal of this research is to investigate the applicability of microfiltration as a reuse/recycling method for semi-synthetic MWFs. This will be accomplished through three specific objectives: (1) to investigate the fouling mechanisms at work during microfiltration of an uncontaminated semi-synthetic MWFs and optimize the

microfiltration system operating parameters to reduce fouling; (2) to investigate the ability of the microfiltration system to remove tramp oil contamination that compromises fluid quality; and (3) to design a semi-synthetic MWF that significantly reduces fouling based on the knowledge gained about membrane fouling mechanisms.

The first objective will be accomplished by studying the mode and intensity of membrane fouling by observing the rate at which three different MWF concentrations foul the microfiltration membranes and the steady-state flux that the system achieves. In addition, Scanning Electron Microscope (SEM) imaging will be used to view the membranes as they become fouled. The data collected in these experiments will be analyzed and conclusions will be drawn about the membrane fouling mechanisms that are present. Transmembrane pressure, cross-flow velocity, and backpulsing are operational parameters that will be studied to determine the effects that they have on membrane fouling once a steady-state flux has been reached with a membrane. This will not only serve to identify appropriate ranges for operation and strategies for optimization but also will serve to further reveal the mechanisms responsible for membrane fouling.

The second objective is to investigate the system's ability to remove contaminants from MWF streams. The applicability of microfiltration in industry is ultimately dependent on how well it eliminates contaminants from the MWF. One primary contaminant in industrial MWF usage is tramp oil. Tramp oils, such as hydraulic oils and way oils, find their way into MWF streams through leaks in fluid systems. These tramp oils can break down the stability of MWFs and have also been shown to increase mist production,

which poses a health hazard. In order to investigate the microfiltration process' ability to remove tramp oil from MWF, a set of experiments will be designed to test removal of two types of tramp oils in varying concentrations of contamination.

The third objective focuses on the design of a semi-synthetic MWF that will significantly reduce the fouling phenomenon when used with microfiltration, based on the principles of component adsorption and repulsive interparticle electrostatic interactions. Fluid composition will be compared with the commonly used semi-synthetic MWF used in the first two objectives. Microfiltration tests will be conducted to determine the fouling behavior of the designed fluid. The fouling and lubricity properties of the fluid will be investigated using both the tapping torque method [15] and a drilling testbed designed for MWF evaluation [16].

The first chapter focuses on intensity and mode during the initial phases of membrane fouling and the effect that operational parameters have on the fouling process. The second chapter addresses the ability of the membrane system to remove tramp oil contamination and the further fouling that occurs due to these contaminants. The third chapter focuses on the development of the novel semi-synthetic MWF that reduces membrane fouling. The final chapter draws conclusions from the research presented within the report.

2. MEMBRANE FOULING OF UNCONTAMINATED SEMI-SYNTHETIC MWF

Membrane fouling is one of the primary concerns that prevent widespread use of microfiltration for semi-synthetic MWFs. Fouling occurs when components within the MWF or contaminating agents block or constrict the pores of the membrane and reduce the system flow rate and lower the quality of the filtered MWF. In order to determine the applicability of microfiltration for semi-synthetic MWFs, the mode and intensity of membrane fouling must be determined. The research presented in this section focuses on determining the fouling characteristics of uncontaminated semi-synthetic MWFs.

MWF concentration's effect on membrane fouling will be investigated. An increase in the fouling rate, or a decrease in end flux reached, along with an increase in concentration, indicates a mechanism that is dependent on the number of particles in contact with the membrane and each other. The effects of transmembrane pressure, cross-flow velocity, and backpulsing will be studied to determine their effects on membrane fouling when the membrane has been fouled to an end flux level. This allows identification of appropriate ranges for operation and strategies for optimization. End flux level is defined as the flux reached at the time that flux decline is replicated within a 24 hr testing period.

2.1 Experimental Plan and Set-up

Two sets of experiments were conducted with a commercial semi-synthetic MWF. The first set investigated the intensity and mode of fouling by following the response of the microfiltration system at MWF concentration levels of 1, 3, and 5% by volume. The

second set of experiments examined the effect of transmembrane pressure, cross-flow velocity, and backpulsing of membrane steady-state flux within the system. The same materials and set-up were used for both sets of experiments.

2.1.1 Membranes

Microfiltration membranes are available in multiple materials, surface chemistries and geometries. There are three main types of materials used in microfiltration: ceramics, sintered metals, and polymerics. The membrane material used in this research was α-alumina, a ceramic chosen for its good thermal stability at elevated temperatures and ability to withstand strong acidic and basic cleaning solutions. Figure 1 provides a Scanning Electron Microscope (SEM) image of the surface of one of the α-alumina membranes used in the experiments at two magnification levels. It also shows the alumina particles that make up the membrane structure.
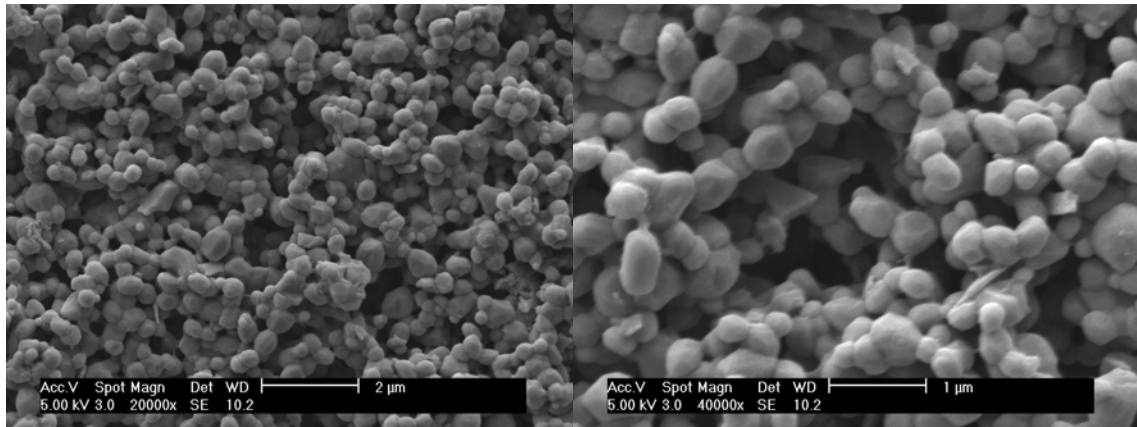
Figure 1 – SEM images of α-alumina membrane at 20000x and 40000x

Two membrane geometries were used in the experiments. A tubular membrane with a length of 250 mm, an outside diameter of 10 mm and an inside diameter of 7 mm

supplied by Pall, Inc. (DeLand, FL) was used in the primary data gathering system. A disk-shaped membrane with diameter of 4.55 cm and thickness of 4 mm supplied by KeraNor AS (Norway) was used in a secondary system to evaluate fouling through the use of SEM imaging. A pore diameter of 0.5 μm that was used in all experiments in order to enable the native semi-synthetic MWF emulsions to pass through the pores while excluding tramp oil emulsions.

2.1.2 Metalworking Fluid

The commercial semi-synthetic MWF studied in this research is commonly used for boring, centerless grinding, cylindrical grinding, internal grinding, reaming, surface grinding, and tapping. The fluid is manufactured by Castrol under the trade name Clearedge 6519 and will be referred to hereafter as the commercial fluid. It is typically diluted to a 3-5% concentration for grinding and a 4-8% for machining. Table 1 provides the MWF components and Table 2 provides pertinent data about the MWF.

Table 1 – Castrol Clearedge 6519 Components

Function	Component	% by wt.
Oil	Napthenic	30-35
Emulsifier	Sulfonate Base	1-5
Emulsifier	Non-ionic (proprietary)	5-10
Corrosion inhibitor	Boric acid	1-5
Biocide/Fungicide	Triazine/pyridiethione	1-2
Diluent	Water	40-60

Table 2 – Castrol Clearedge 6519 Properties

Concentrate Appearance	Viscous Dark Blue Fluid
Diuted Appearance	Translucent Blue Fluid
Viscosity @ 20C	0.998 cP
Particle Size	32 nm
Zeta Potential	-64 mV
pH	9.3

The MWF emulsions were created by adding a pre-measured amount of concentrate to a beaker of water that had been purified to 18MΩ resistivity. The MWF concentrate was distributed throughout the water by a magnetic stirrer.

2.1.3 Experimental Systems

Three microfiltration membrane systems were used in this research. The majority of the work was accomplished using a tubular membrane system with an attached backpulsing unit, referred to subsequently as the "main system". A second tubular membrane system was used to wash membranes and is referred to as the "cleaning system". The final system used in the research was a disk membrane system used to prepare membranes for viewing with Scanning Electron Microscopy (SEM). It is referred to as the "disk system".

The main system was used to collect flux data from the microfiltration tests. Unless otherwise specified, all flux data presented in this report was collected on the main system. The main system is shown in Figure 2 and schematically in Figure 3. The MWF was held in a 5-liter steel process tank and fed into the inlet port of a Membralox membrane module by a 1 hp gear pump controlled by a Motor Master 20000 Series (Minarik Corp. Glendale, Ca). Temperature data was recorded by a thermometer. The

pressure entering (P_1) and exiting (P_2) the membrane module was measured by two 1 bar pressure gauges. The transmembrane pressure was calculated by taking the average of these two pressures. The pressure was adjusted with a ball valve that followed the membrane module. Backpulsing was provided by a Declomatuer BF3 Backflush unit fed by compressed nitrogen at 6.90 bar. Flux was measured by opening the permeate valve of the membrane housing and recording the volume of permeate with a computer-based data collection program.

Figure 2 – Main System
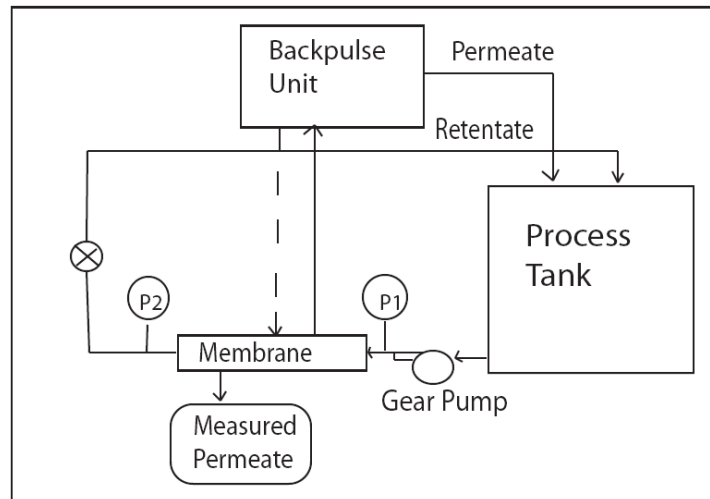
Figure 3 – Main System Schematic

The cleaning system was used to wash membranes with various surfactants and to test for fouling reversibility. The cleaning system is shown in Figure 4. The system is similar to the main system. The main difference between them is that the cleaning unit lacks a backpulsing system. The flow in the cleaning system is driven by a 0.5 hp gear pump. The same membrane housing type is used in both the cleaning system and the main system. This facilitates transfer between the systems for membrane washings. A heating coil was used in conjunction with a thermometer to keep the cleaning solutions at the correct temperature.

Figure 4 – Cleaning Test-Bed

The third system was used to prepare samples for viewing in the SEM. A separate system was necessary for this because the tubular membranes could not be viewed by SEM without destroying them. A disk membrane system was chosen for this task because it has a flat surface that allows for easy SEM viewing and low cost relative to the tubular membranes. The disk membrane system is shown in Figure 5. A 500 ml fluid reservoir was used to contain the fluid. The flow was driven by a gear pump. An acrylic membrane housing was fabricated to allow cross-flow conditions. The housing composed of two halves. The base half holds the membrane in a recess. The other half contains a channel that allows the fluid to flow across the face of the membrane. It also contains a pressure gauge to measure transmembrane pressure. A custom Viton gasket was fabricated to ensure the seal between housing halves. The material was chosen for its low reactivity with the MWF components. Figure 6 provides an image of the membrane housing.
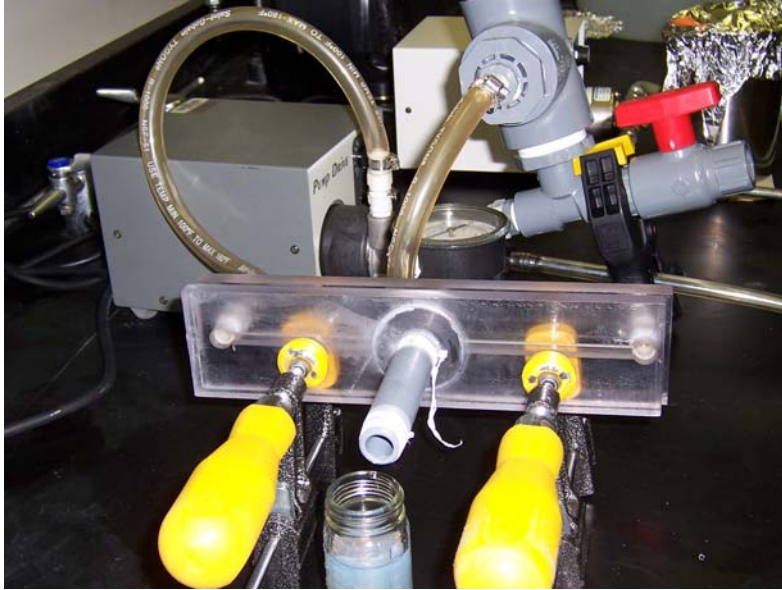
Figure 5 – Disk Membrane System

Figure 6 – Disk Membrane Housing

2.2 Intensity and Mode of Membrane Fouling

2.2.1 Experimental Procedure

The membrane fouling rate and the end flux level was investigated at three concentrations. The concentrations (1%, 3%, and 5% by volume) were made by dilution in ultrapure water. Prior to running experiments, the purity of the system was verified by running a cleanliness check using a conductivity meter. This was accomplished by testing the conductivity of ultra-pure (18 MΩ) water before and after running it through the system. If the two readings matched, the experiment could begin. If they did not match, the system was flushed until the resistivity of both samples matched.

The second step in the experimental procedure was to measure the clean water flux (CWF) of the membrane used in the test. The operational parameters were a cross-flow velocity of 6.0 m/s, a transmembrane pressure of 0.255 bar, backpulsing at a frequency of 2 min for a duration of 1 s, and a 5 L sample volume in the process tank. The CWF was determined to be the steady-state flux reached by the membrane. The steady-state was typically reached within 30 min. If not, it was assumed that there was a contaminant in the system that was causing membrane fouling and the system and membrane were both re-cleaned prior to the test. Figure 7 shows a typical flux curve of a CWF test. The flux increase seen in the first couple of minutes is thought to be caused by the wetting kinetics of the membrane pores. The larger pores are wetted most easily, while the smaller pores being wetted and allowing flow later. As more pores are wetted, they allow flow through them and the flux increases until all pores are wetted.
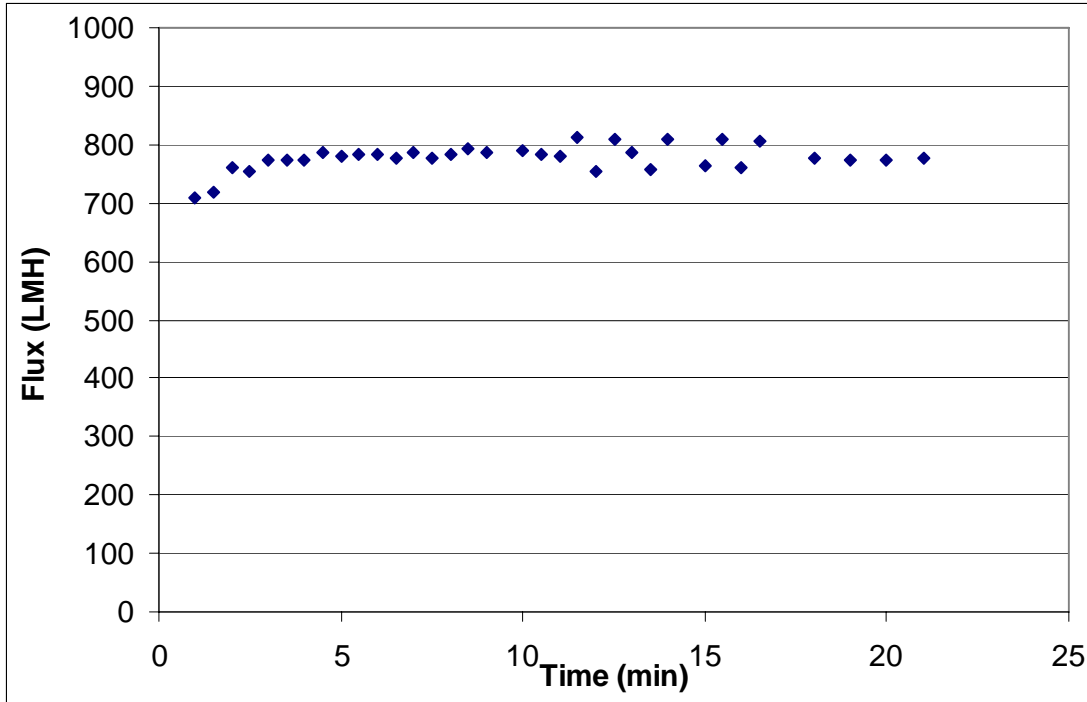
Figure 7 – Typical CWF Test Flux Results

Once the CWF of the membrane has been established, the system is drained and the process tank filled with 5 L of the test fluid. All of the tests on the effect of MWF concentration were conducted with the same operating conditions: 0.255 bar transmembrane pressure; 6.0 m/s cross-flow velocity; and backpulsing at a frequency of 2 min for a duration of 1 second per pulse. Flux measurements were taken at 5 minute intervals and membrane surfactant washes were conducted every 24 hrs.

A second measurement of success in the applicability of microfiltration of semi-synthetic MWFs is the transmission of the fluid components through membrane pores. This was measured through the use of the refractive index. Samples of MWF concentrations between 0% and 10% were measured for refractive index and a chart of MWF

concentration vs. refractive index was created (Figure 8). Permeate and retentate samples taken during the tests were matched against the chart to check for change in MWF micro-emulsion concentration between the samples. There is a linear relationship exhibited between the MWF and the refractive index within the concentrations investigated in this research. To calculate the percentage of MWF micro-emulsions that are transmitted through the membrane pores, the concentration of the MWF permeate is divided by the concentration of the MWF retentate. If the two concentrations are the same, then it is assumed that the fluid is fully transmitting through the membrane.
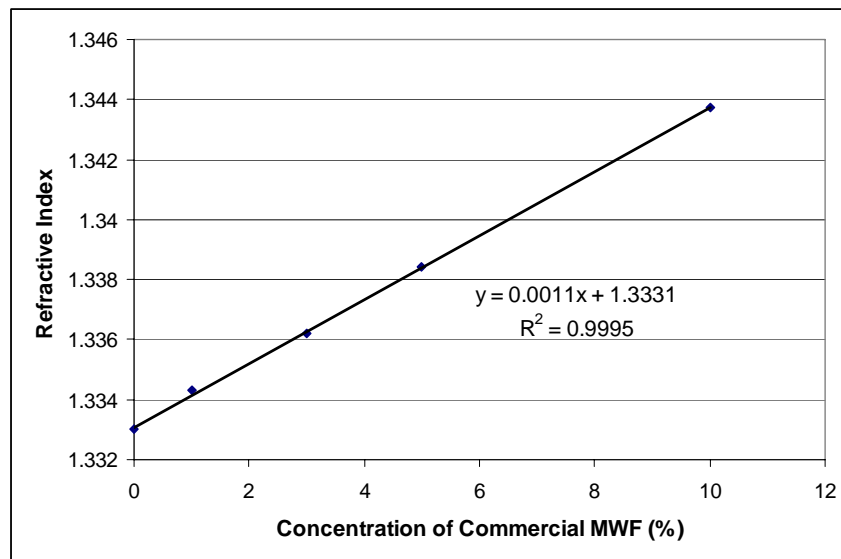
Figure 8 – Refractive Index vs. MWF Concentration

Two cleaning procedures were used in this research. The first cleaning procedure, membrane surfactant washing, was used in tests on the mode and intensity of membrane fouling. The second cleaning procedure, membrane cleaning by pyrolysis, was used to

regenerate fouled membranes to the state of a new membrane so that they could be used in other tests.

The surfactant cleaning procedure was designed to remove reversible fouling from fouled membranes and reveal irreversible fouling. The surfactant cleaning procedure consists of four steps. The first step is to drain the test fluid and recirculate DI water at 50°C for 1 hour. The second step is to move the membrane to the cleaning system and add a solution of 2% Dawn dish detergent. This solution is recirculated at 80°C for 1 hour to reemulsify any oil that may have coalesced. The third step is to clean the system itself without the membrane by using a new batch of the same membrane cleaning solution. This step removes any oil that has deposited within the tubing of the system. The final step is to drain the surfactant solution and rinse the membrane and system until clean. The membrane and system are determined to be clean by using the same criteria as before the beginning of a test; namely that a conductivity meter reads the same for ultra-pure water before and after being cycled through the system. Results for this cleaning procedure and for other cleaning agents that were tried are provided in Appendix A.

The pyrolysis cleaning procedure was used to regenerate fouled membranes to the state of a new membrane. This procedure involves heating the membrane to 800°C at a rate of 8°C/min and dwelling for 3hrs. The oven is then allowed to cool for about 24 hrs when the interior temperature reaches 30°C. The rate of heating and cooling in this process is extremely important due to the nature of the ceramic membranes. Thermal cracking can occur microscopically and therefore is not always easily detected. This can create

fissures on the membrane surface that are orders of magnitude larger than the nominal pore size. The rate of thermal change was therefore kept below the manufacturer recommended 9°C/min. This cleaning procedure was extremely effective in removing any type of organic foulant such as MWFs or the contaminants often found within them. Table 3 provides before and after flux data for four pyrolysis cleanings of the same membrane following fouling tests. It can be seen from the table that the pyrolysis cleaning technique is able to fully restore the membrane to its initial state as indicated by clean water flux.

Table 3 – Before and After Flux Data for Pyrolysis Cleaning

Pyrolysis Cleaning Efficiency				
Cleaning #	Temp	CWF (LMH)		Efficiency
		Before	After	
1	800	277	979	1.00
2	800	391	940	0.93
3	800	594	986	1.02
4	800	440	901	0.86
Original CWF = 979 LMH				

2.2.2 Results for Membrane Fouling Tests

The flux results for the fouling tests are shown in Figures 9-11, which demonstrate the flux response of the three different concentrations as a function of filtration time. The permeate flux decline seen in these figures results from the fouling of the membrane and the slope of the flux decline is a measure of the fouling rate.
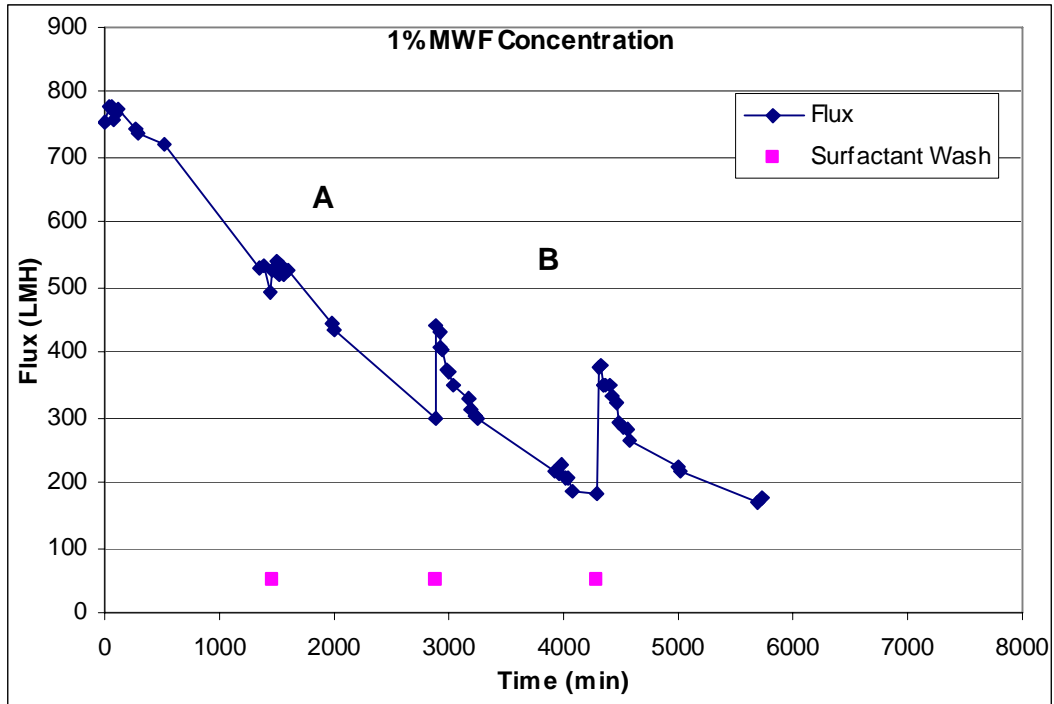
Figure 9 – Flux of 1% MWF Concentration
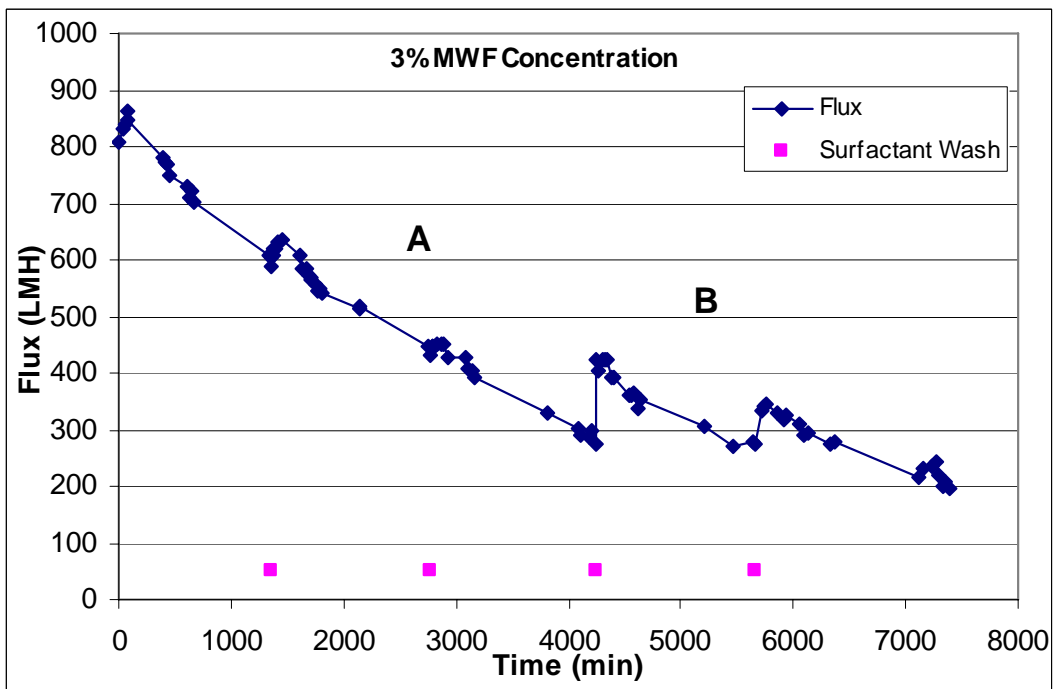
Figure 10 – Flux of 3% MWF Concentration
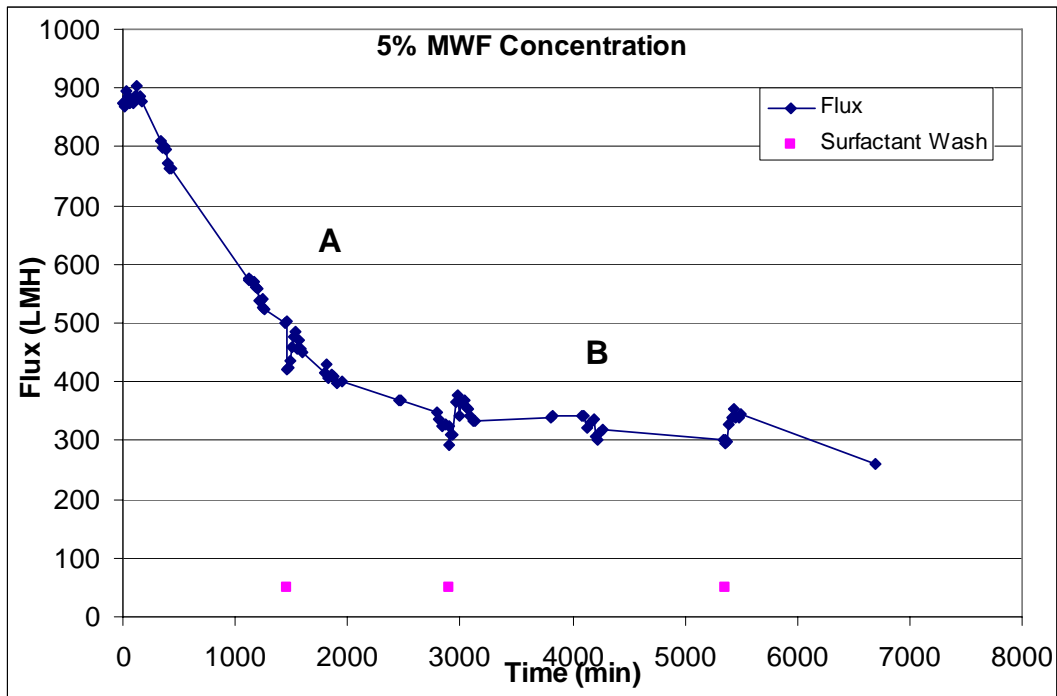
Figure 11 – Flux of 5% MWF Concentration

Figures 9-11 shows that the MWF concentration does not have a significant effect on the final flux level reached, i.e., the flux levels are quite similar after 6000-7000 minutes. However, there is a significant difference in the manner by which the three concentrations reach this final flux level.

The fouling for each concentration is divided into two stages. The first stage ("A") takes place over approximately the first 3000 minutes and exhibits a linear decrease for the 1% and 3% concentrations and a quadratic decrease for the 5% concentration. The second stage of fouling ("B") exhibits a continued decrease in flux with a saw-tooth pattern

consisting of the flux jumping suddenly and then decreasing slowly. This saw-tooth pattern decreases in magnitude as the MWF concentration increases.

The saw-tooth pattern of region "B" is explained by the fact that the jumps in the flux correspond with surfactant washings. Figures 9-11 shows that this correlation is present in both stages of the membrane fouling but is more marked in region "B". The reason for this lies with two fouling phenomena responsible for decline in flux over time: pore constriction due to aggregate formation and deposition and the formation of a cake layer of particles on the membrane surface. Both of these mechanisms can be happening at a given time. It is the predominance of one mechanism over another that determines whether the membrane is in stage "A" or stage "B" of fouling. Once critical coverage of the membrane has taken place then a cake composed of particles depositing on previously deposited particles is formed.

2.2.3 Discussion of Fouling Mechanism Experiments

The deposition of oil particles on the membrane surface is hypothesized to be due to inertial forces that push the particle toward the surface overcoming the electrostatic repulsive forces between the particle and membrane surface. In the system used in the current research, the surface potential of the particles is more strongly negative than the potential of the α-alumina membrane. This leads to a lesser repulsive force that must be overcome between the particle and the membrane than between two particles. Therefore, the cake layer formed by interparticle interactions is more easily reversible than the deposited layer. This is supported by the saw-tooth behavior of region "B" in Figures 9-

11 that shows the cake layer being reversed by surfactant washing while leaving the deposited layer on the membrane.

Figures 12-14 illustrates the fouling process. When the filtration process begins, there is deposition (Fig. 12) with a small amount of cake layer formation. When the membrane with only the deposited layer is washed, the particles are not re-entrained into the flow because the repulsive force between the micro-emulsions and the membrane is too strong. Therefore, a smaller jump in flux following a membrane washing is observed in region "A" than in region "B". As the deposited layer on the membrane is created, a cake layer forms on the top (Fig. 13). When this occurs, the magnitude of the jump in flux following surfactant washing increases relative to region "A" because the particle-particle forces are weaker than the particle-membrane forces. The particles forming the cake layer are re-entrained into the flow by the re-emulsification action of the excess surfactant (Fig. 14).
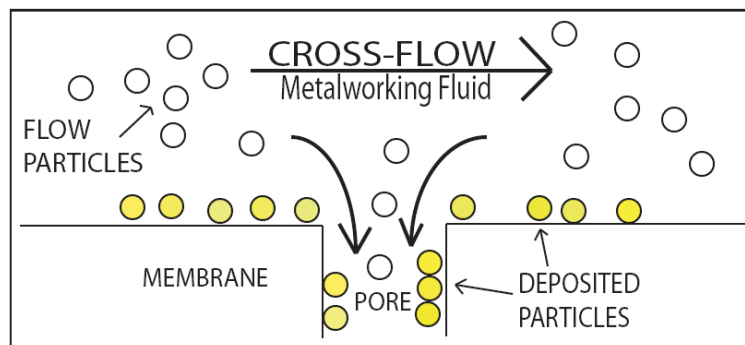
Figure 12 – Illustration of Membrane Fouling by Particle Deposition
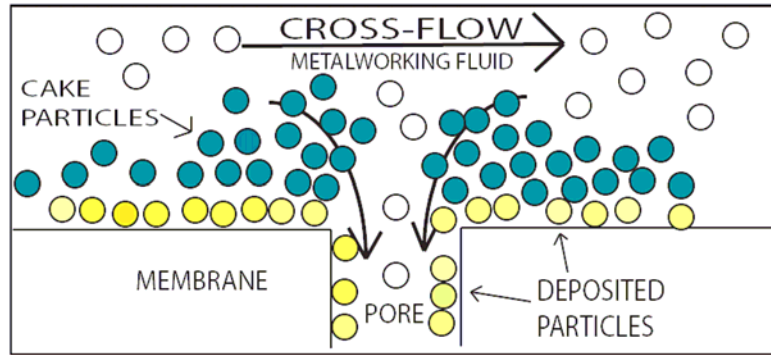
Figure 13 – Illustration of Membrane Fouling by Cake Layer
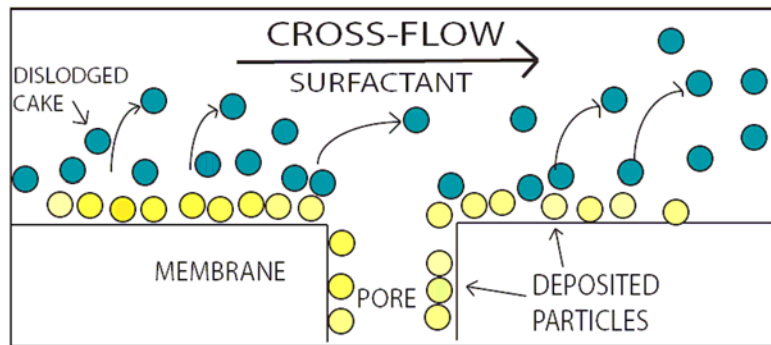
Figure 14 – Illustration of Membrane Cleaning by Surfactant Washing

Further evidence for deposition as the initial fouling mechanism is demonstrated by plotting the hydraulic resistance of the membrane versus time as the membrane fouls. Mueller et al. [17] used a resistance model to describe the transport of fluid through the membrane due to transmembrane pressure as follows:

$$R_t = R_m + R_f = R_m + R_{if} + R_{ef} = \frac{\Delta P}{v_p J} \qquad (1)$$

where R_t is the total resistance, R_m is the intrinsic membrane resistance, R_f is resistance due to fouling and is made up of internal fouling (R_{if}) and external fouling (R_{ef}), ΔP is the transmembrane pressure, v_p is the kinematic viscosity and J is the permeate mass flux.

Mueller et al. [17] and Tracey et al. [18] describe how a plot of the total resistance versus time can provide insight into the specific method of fouling. This is due to the form of the equations used to model each fouling mechanism.

In the case of internal fouling (pore constriction and pore blocking), R_m increases with time. The equation provided by Tracey et al. [18] for pore constriction is

$$R_m = R_0 \left(1 + K_{PCM} Q_0 t\right)^2 \qquad (2)$$

where R_0 is the initial membrane resistance, Q_0 is the initial volumetric permeate flow rate, K_{PCM} is a rate constant, and t is time. A plot of this curve versus time will yield a curve that is concave up.

In the case of external fouling (cake formation) the equation provided by Tracey et al. [18] is

$$R_m = R_0 (1 + 4t K_{CFM} Q_0^2)^{0.5} \qquad (3)$$

with similar nomenclature to Equation 2. A plot of this curve versus time will yield a curve that is concave down. Thus, a resistance curve that is concave up indicates internal fouling and a concave down curve indicates external fouling.

Equation (1) was used to convert the flux data from Figures 9-11 into total resistance data. Figure 15 shows the resistance curve for 1% MWF concentration. The resistance curve is split into the same two stages as the flux curves. The first stage ("A") is clearly upwardly concave, showing that the initial fouling is due to internal fouling. The second stage of the curve ("B") shows a downward concavity that represents external fouling.
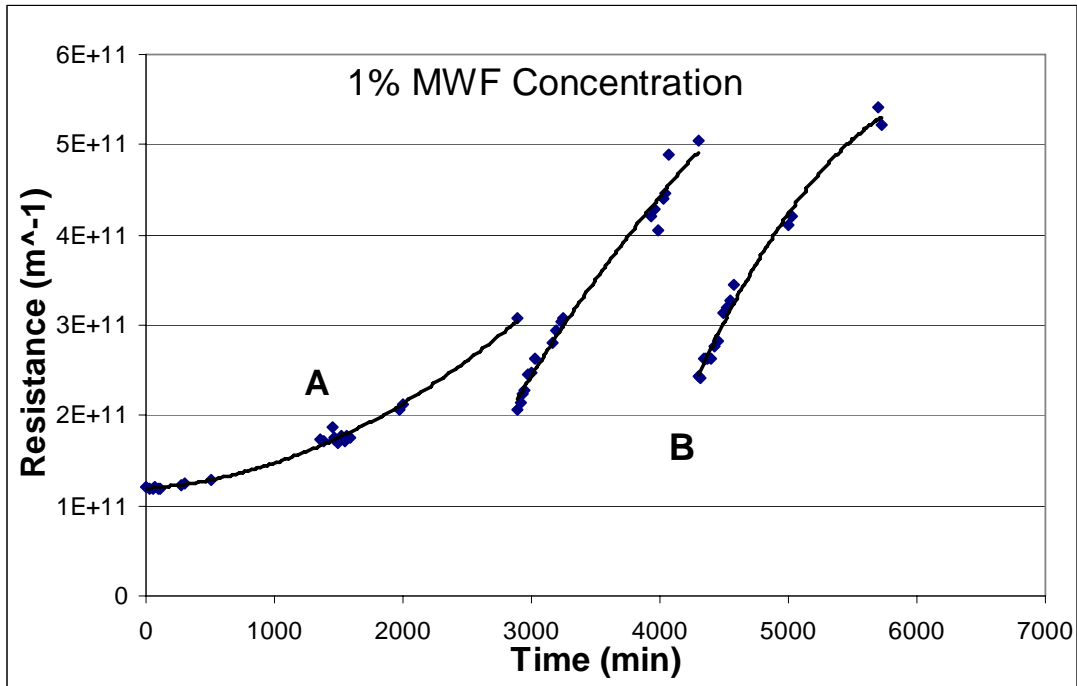
Figure 15 – Resistance Curve for 1% MWF Concentration

SEM imaging was used to provide further insight into how the membrane fouling occurs. Figure 16 shows a new membrane under 20000X magnification that has not been exposed to MWF. The spherical objects shown in the image are the alumina particles that make up the membrane structure. Figure 17 shows a membrane that has been fouled by a 5% concentration of MWF to a region near the end of region "A", as indicated in Figure 11. Figure 17 illustrates the fouling mechanism of pore constriction by aggregate deposition. Examples of deposited particle aggregates are circled in the image. The smaller spherical shapes in the figure are the micro-emulsions that have been deposited in an aggregate on the alumina membrane. The relatively open structure of the membrane has been severely closed in by the deposited particles thereby constricting the pore

openings. A more magnified view of some of the deposited aggregates is provided in Figure 18. Figure 19 shows a membrane that has been fouled into region "B" of Figure 11. This figure illustrates the formation of the cake layer. The cake layer is the large aggregate network of particles that appears to be draped over the membrane structure and obscures the pores beneath. These images provide further evidence that the membranes are fouled by a deposited layer of particles that constrict the pore openings. This is followed by the formation of a cake layer formed of aggregate clusters of particles. Figure 20 shows a membrane that has been fouled into region "B", followed by a surfactant washing. A more comprehensive group of SEM images for each of the membrane states has been provided in Appendix B.
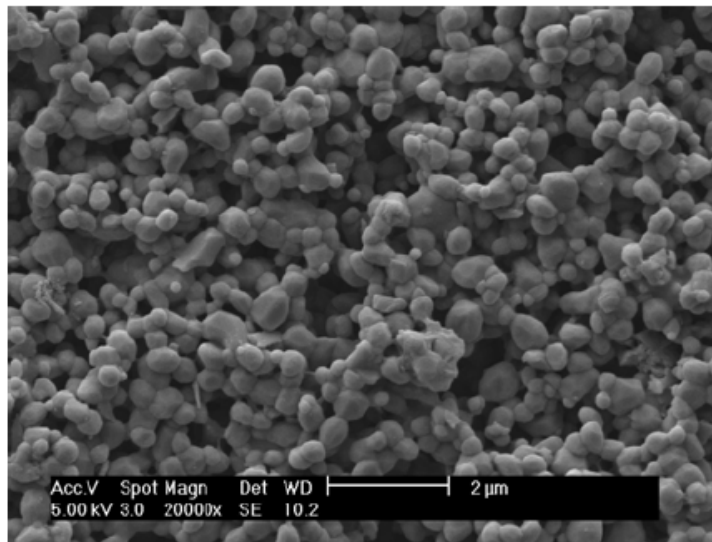
Figure 16 – SEM Image of Clean Membrane (20000X)
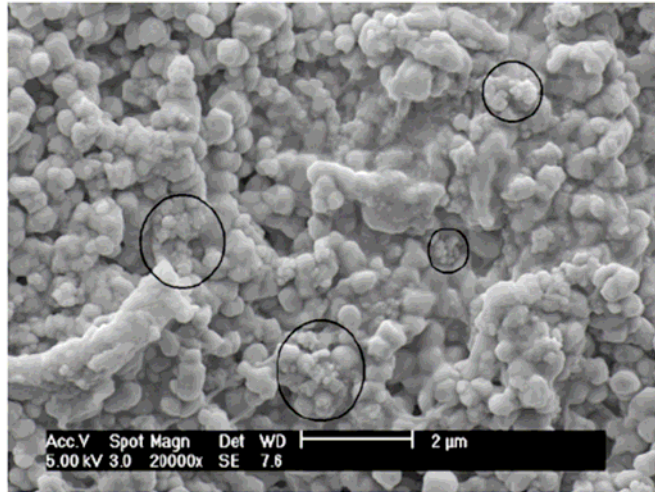
Figure 17 – SEM Image of Fouled Membrane Showing Particle Deposition (20000X)
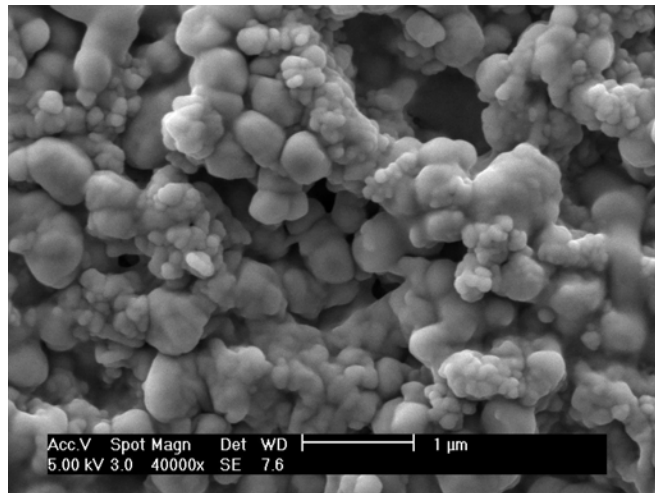
Figure 18 – SEM Image of Fouled Membrane Showing Particle Deposition (40000X)
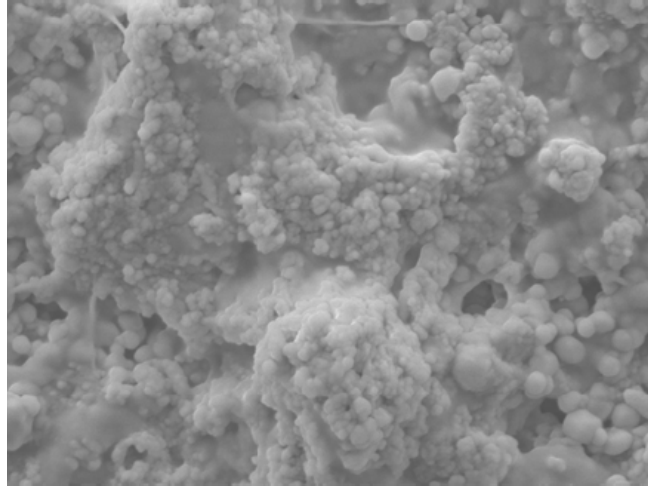
Figure 19 – SEM Image of Fouled Membrane Showing Cake Layer (20000X)
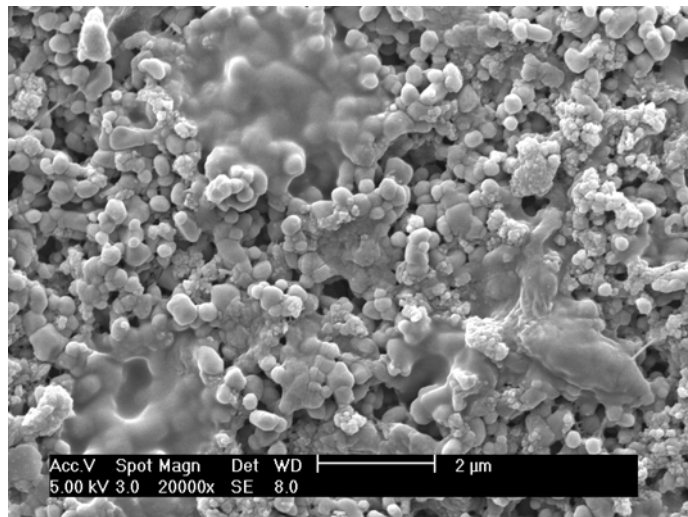
Figure 20 – SEM Image of Membrane Following Surfactant Washing (20000X)

2.3 Effect of Operational Parameters on Membrane Fouling

In Section 2.2, it was shown that the initial stages of fouling by deposition are irreversible. However, the latter stages of fouling, by the creation of a cake layer, are reversible through surfactant washing. This indicates that a weaker force holds the cake layer together and suggests that the formation of the cake layer might be either slowed or

reversed by other means. The operational parameters of the microfiltration system are a natural place to start investigating these other means.

2.3.1 Experimental Methodology

A 2^3 factorial experiment was conducted to examine the effects of transmembrane pressure, cross-flow velocity, and backpulsing on membrane fouling. The test conditions are summarized in Table 4 along with the randomized order of the tests. The initial state of the membrane was reached by processing a 5% of MWF at a transmembrane pressure of 0.255 bar; a cross-flow velocity of 6.0 m/s; and backpulsing at a frequency of 2 minutes for a duration of 1 second until the system reached a steady-state.

Table 4 – Test Levels for Operational Parameters Experiment

2^3 Factorial Experiment Levels				
Test #	Test Order	Pressure	Velocity	Backpulse
		(psi)	(m/s)	
1	2	4	2.5	off
2	3	10	2.5	off
3	5	4	6	off
4	1	10	6	off
5	4	4	2.5	on
6	8	10	2.5	on
7	6	4	6	on
8	7	10	6	on

The experiments were conducted by running the system at a base level until the flux reached steady-state, changing the variable to the specified levels for a given trial, and running the test until a new steady-state flux was achieved. This flux was then recorded as the response for the test. The settings were then reset to the baseline level and the flux

recorded again. The replicated measurements of the baseline flux were also used to determine the experimental error used in the statistical analysis of significance.

2.3.2 Results of Operational Parameters Testing

The flux results are shown in Figure 21 and in Table 5. The baseline flux before and after each trial is signified by open boxes in Figure 21. Because the baseline flux values are all close to 160 LMH, it can be concluded that all changes brought about by the variable level changes are reversible. This implies that the effects seen in this experiment are the result of a fouling structure caused by the operating conditions.
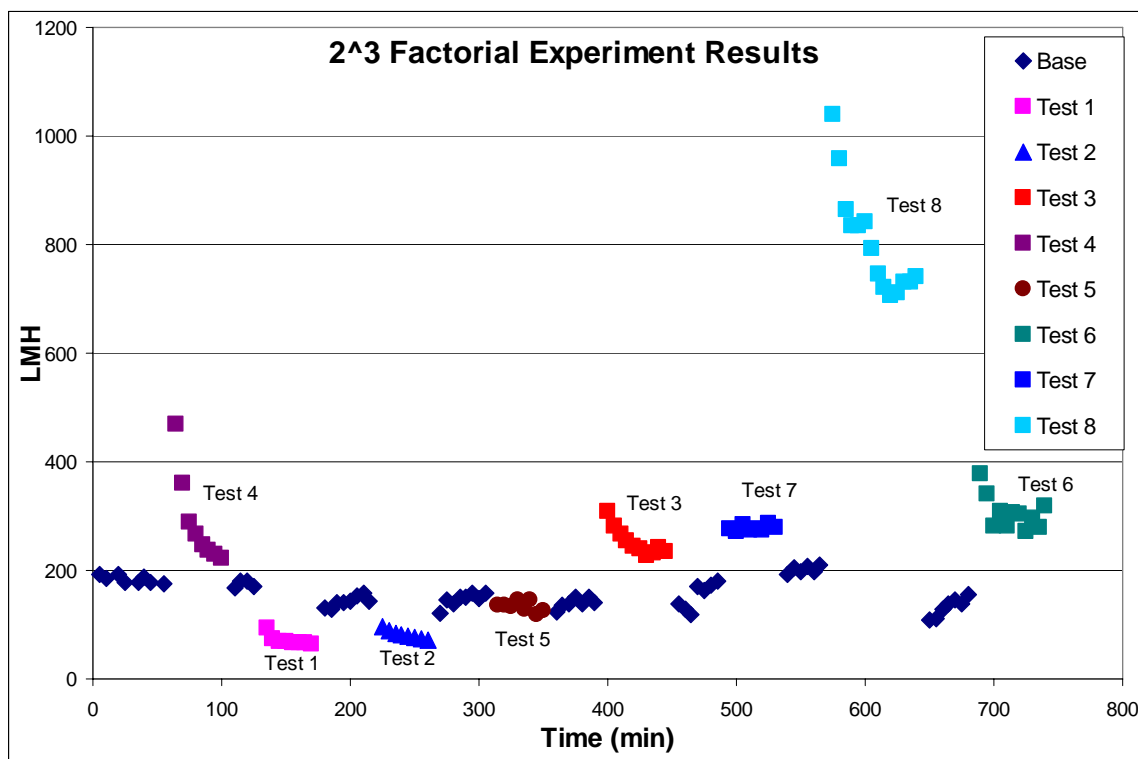
Figure 21 – Results of 2^3 Factorial Experiment

Table 5 – Levels and Responses of Experiment on Operational Variables

2³ Factorial Experiment Levels and Responses					
Test #	Pressure	Velocity	Backpulse	Baseline Flux	Flux
	(bar)	(m/s)		(LMH)	(LMH)
Baseline	0.26	6	on	162.6	162.6
1	0.28	2.5	off	171.2	64.7
2	0.69	2.5	off	157.4	72.5
3	0.28	6	off	149.9	235.5
4	0.69	6	off	177.6	222.1
5	0.28	2.5	on	158.4	125.5
6	0.69	2.5	on	145.8	317.3
7	0.28	6	on	172.3	278.0
8	0.69	6	on	207.5	740.2

The results of the statistical test of significance are shown in Table 6. A normal probability plot of the effects demonstrated the need for a data transformation. This was accomplished by taking the natural log of the data. The data indicate that the three main effects of transmembrane pressure, cross-flow velocity, and backpulsing are all statistically significant. Among interactions, only the 2-factor interaction between transmembrane pressure and backpulsing is significant, based on a confidence interval with and α-level of 0.05.

Table 6 – Statistical Analysis of Experiment on Operational Variables

Confidence Interval Analysis				
Effect		Estimate	95% C.I.	Significant
Pressure	1	0.490521	± 0.30317	yes
Velocity	2	1.01347	± 0.30317	yes
Backpulsing	3	0.877127	± 0.30317	yes
Pres X Vel	1*2	-0.030163	± 0.30317	no
Pres X BP	1*3	0.4629	± 0.30317	yes
Vel X BP	2*3	-0.192276	± 0.30317	no
Pres X Vel X BP	1*2*3	0.056041	± 0.30317	no

2.3.3 Discussion of Operational Parameters Testing

The results of the operational parameters testing indicate that a decrease in cross-flow velocity decreases flux. This reinforces the previous conclusion that the membrane flux under steady-state flux conditions is limited primarily by a porous cake layer rather than the membrane pore structure itself. If the flux was limited by internal pore constriction, then a change in cross-flow velocity should have no effect on the flux because the deposits within the pores cannot be remobilized by the cross-flow. However, if the membrane fouling were caused by a build-up of an aggregate porous structure on the membrane surface, then an increased cross-flow velocity would be expected to increase the flux because of the increased shear forces working to sweep away the fouling cake.

Figures 22-24 show the two-way diagrams of the statistical analysis for the operational parameters testing. Figures 22-23 show that there is no significant interaction between transmembrane pressure and cross-flow velocity or cross-flow velocity and backpulsing. Figure 24 shows the two-way diagram of the transmembrane pressure and backpulsing interaction effect. It indicates that flux is independent of transmembrane pressure when backpulsing is off, but increases along with increasing transmembrane pressure when backpulsing is on. This result is similar to what Lee et al. [19] reported for fouling by a gel layer in ultrafiltration when processing soluble oil in the absence of backpulsing. They reported that, after a certain amount of time, the membrane flux became almost independent of pressure and that increasing the pressure only served to thicken the gel layer without affecting the flux. At higher pressures, the introduction of backpulsing is much more effective than at lower pressures as seen by the data in Table 6. This is to be

expected because when the transmembrane pressure is high, the permeate drag force pulling the particles to the membrane surface is strong and a denser porous cake would be expected to form.
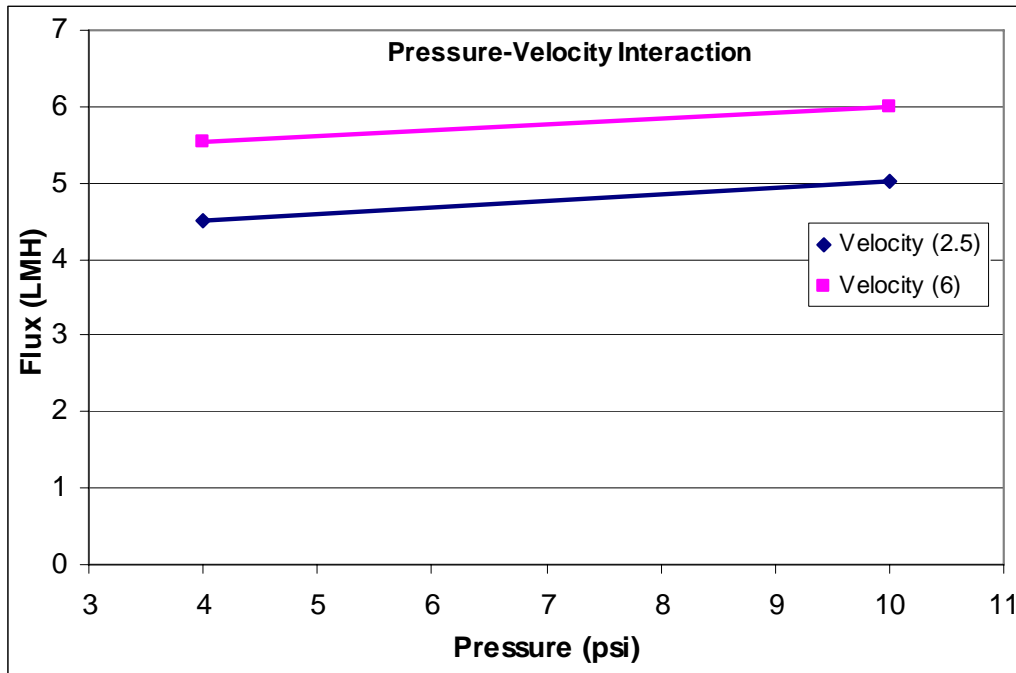
Figure 22 – Two-Way Diagram of Transmembrane Pressure and Cross-Flow Velocity

Interaction
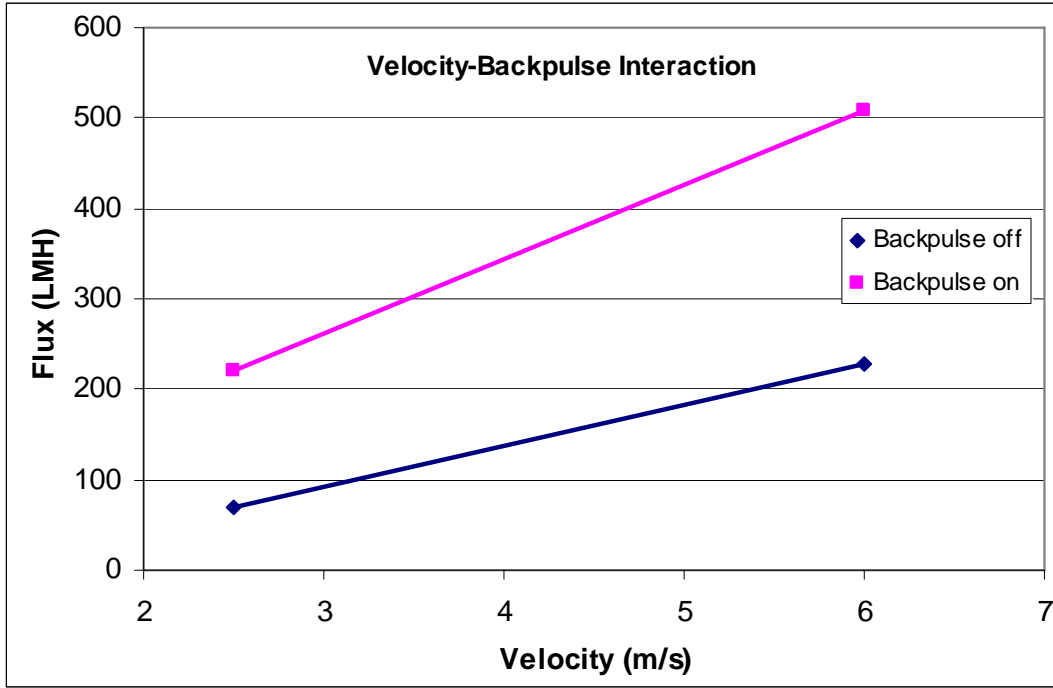
Figure 23 – Two-Way Diagram of Cross-Flow Velocity and Backpulsing Interaction
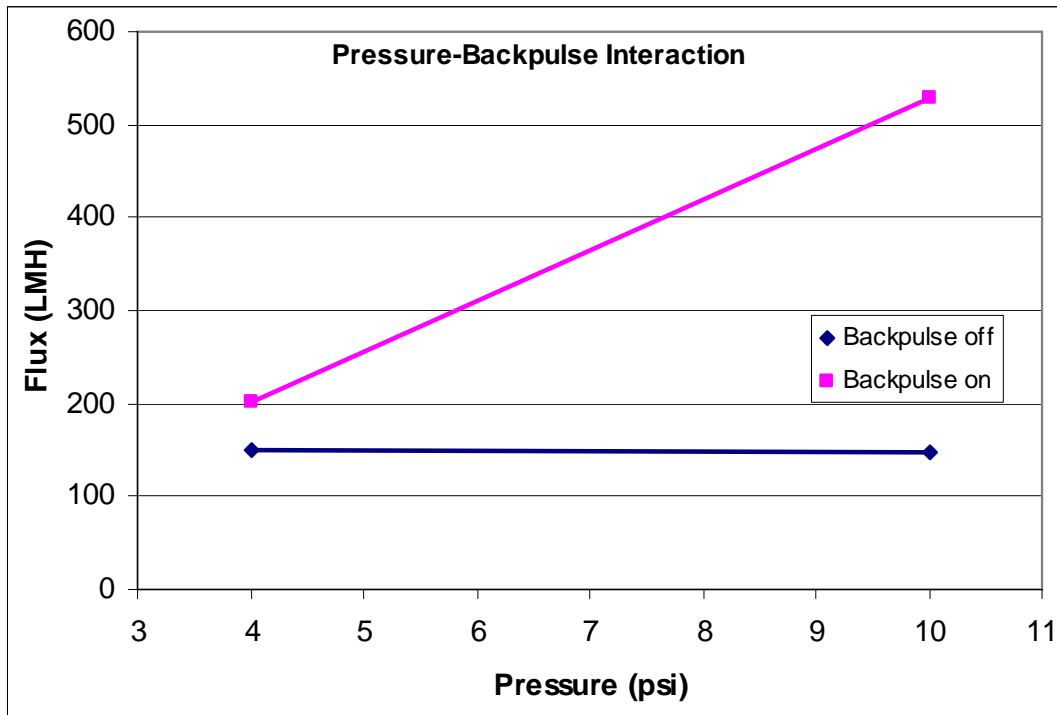
Figure 24 – Two-Way Diagram of Transmembrane Pressure and Backpulsing Interaction

The interaction effect of transmembrane pressure and backpulsing is highly instructive. Backpulsing would only be expected to be effective if there was a dense porous cake layer obstructing access to the pores. A very loose porous structure would not be expected to be significantly perturbed by backpulsing due to rapid pressure dissipation through the open channels of the porous structure. Figure 25 compares a membrane being fouled with backpulsing with one that is being fouled in the absence of backpulsing. Both tests were conducted at high velocity and low pressure. The similarity of the two flux curves imply that when operating conditions are conducive to formation of a loose porous fouling structure (high cross-flow velocity and low transmembrane pressure), then backpulsing is not effective.
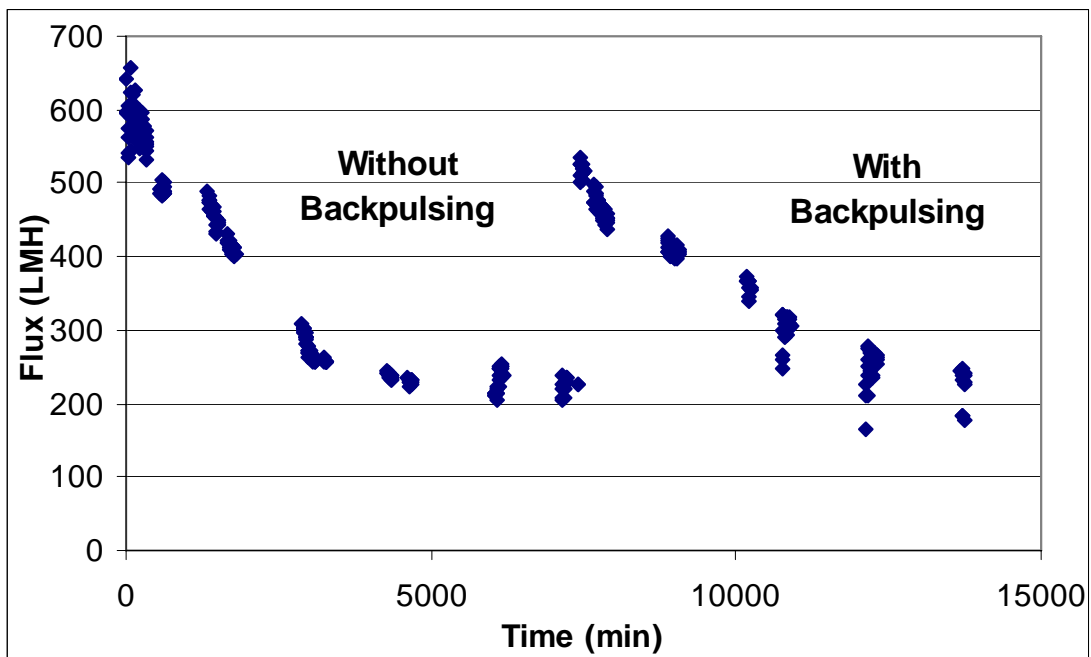
Figure 25 – Membrane Fouling With and Without Backpulsing

47

2.4 Summary of Membrane Fouling of Uncontaminated Semi-Synthetic MWF

The following points summarize the research addressed in this chapter:

1. Within the concentration levels tested, 1%-5%, the concentration of an uncontaminated semi-synthetic MWF does not have an effect on the end flux level reached in microfiltration.

2. For a given set of operating parameters, membrane fouling occurs first by deposition of particles on the membrane and then by the formation of a cake layer.

3. Fouling that occurs when a cake layer is formed can be reversed, to a certain extent, by surfactant washing and changes in the operating parameters.

4. In the presence of a cake layer, flux is responsive to changes in transmembrane pressure only in the presence of backpulsing. In the absence of backpulsing, flux is dependent on cross-flow velocity.

5. Backpulsing is most effective for systems that are run at high transmembrane pressures.

3. MEMBRANE FOULING BY TRAMP OIL CONTAMINATED SEMI-SYNTHETIC MWFS

The previous section showed that uncontaminated semi-synthetic MWFs contribute to membrane fouling through micro-emulsion aggregate deposition followed by cake layer formation. However, the MWFs used in industry are never in an uncontaminated state, so the applicability of microfiltration in industry is ultimately dependent on how well it eliminates contaminants from the MWF. A primary contaminant in industrial MWFs is tramp oil, such as hydraulic and way oils. These oils find their way into MWF streams through leaks in fluid systems. They can break down the stability of MWFs and have also been shown to increase mist production, which creates a health hazard. In order to investigate the ability of the microfiltration process to remove tramp oil from MWF and the further effect that tramp oils have on membrane fouling, a set of experiments was designed to show flux behavior and removal efficiency of two types of tramp oils in varying concentrations of contamination.

3.1 Experimental Materials

The membrane system used in this research is the same as described as the main system in Section 2.1. The membranes used were the same type of tubular α-alumina membranes as in Section 2.1. The same semi-synthetic MWF was used for this testing as in the previous sections. The model contaminants used in this research were hydraulic oil (Mobil DTE, Exxonmobil) and way oil (Way Lube, CLC Lubricants).

3.2 Experimental Plan and Method

The experimental plan consisted of a set of four experiments to foul membranes with hydraulic and way oils. Table 7 shows the fluid and contaminant used in each of the experiments. There were two types of experiments conducted. The first consisted of a constant concentration of contaminant within the system. The second type involved increasing the contaminant concentration with time. The control experiment was conducted with no fluid contamination and is the same experiment as described in Section 2.2 for a 5% MWF without surfactant washings.

Table 7 – Fluid Contaminants and Experiments

Test No.	Hydraulic Oil Concentration		Way Oil Concentration	
	Start	End	Start	End
1	1.0%	3.0%	0.0%	0.0%
2	1.0%	5.0%	0.0%	0.0%
3	1.0%	2.0%	0.5%	1.0%
4	0.0%	0.0%	0.0%	0.0%

Fluid contaminants were introduced into the MWF through the use of a gear pump. One liter of MWF was mixed with the entire contaminant volume by running it through a 0.5 hp gear pump until the tramp oil was fully emulsified, as indicated by the creamy, opaque appearance of the fluid. This mixed fluid was then added to the remaining 4 liters of the MWF within the process tank. For tests where the concentration of tramp oil was increased during the test, a liter of the test fluid was removed from the process tank. The additional tramp oil was emulsified within this portion through the use of the gear pump prior to reintroduction to the process tank.

The operating parameters for the tramp oil tests were the same as for the concentration effect experiments outlined in Section 2.1. The tests were conducted with a transmembrane pressure of 0.255 bar, a cross-flow velocity of 6.0 m/s and a 1 second backpulse at an interval of 2 minutes. The system flux was measured at 5 minute intervals and permeate and retentate samples were taken periodically to test for transmission of tramp oil through the membrane pores.

The level of tramp oil rejection by the microfiltration membrane was measured through the use of UV-Vis spectroscopy. Samples of MWF contaminated with concentrations of tramp oil varying from 0 to 500 ppm were created and measured for absorbance using UV-Vis spectroscopy. The samples were used to create tramp oil concentration vs. absorbance curves that can be used to determine the amount of tramp oil concentration within the permeate and retentate samples. These curves are shown in Figure 26. Each curve represents a different wavelength from 350 to 550 nm.
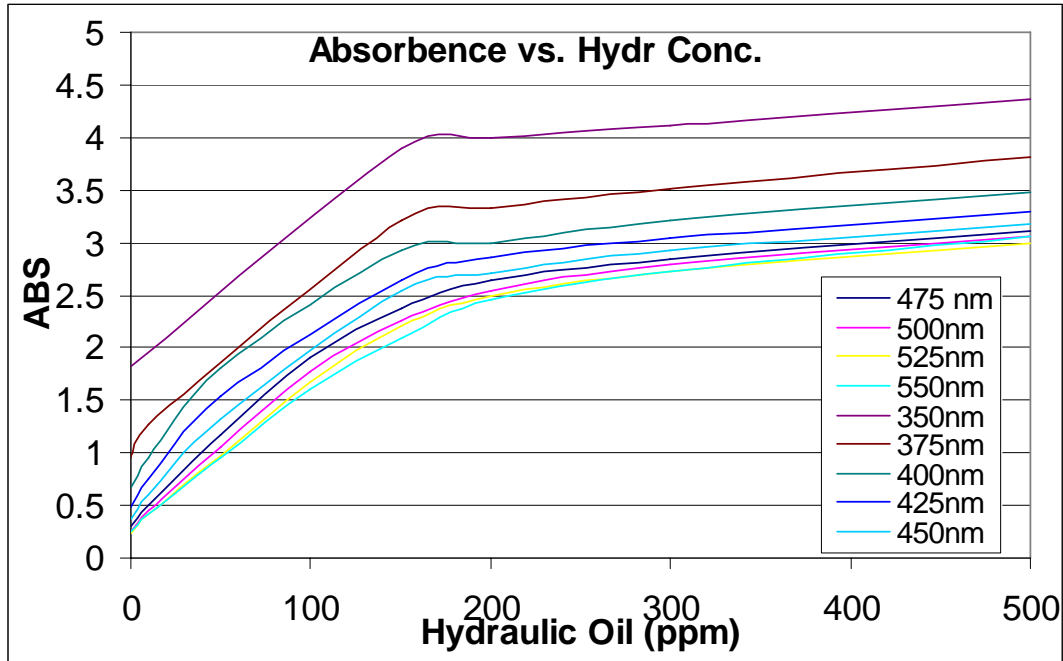
Figure 26 – Absorbance vs. Hydraulic Oil Concentration

Due to the nature of the absorbance measurements, concentrations of hydraulic oil above about 550 ppm are difficult to differentiate from each other. All of the retentate samples have tramp oil concentrations well above this threshold. Therefore, the retentate tramp oil concentration is assumed to be the concentration that was originally created for the test. The highest tramp oil concentration found within the permeate samples was 433 ppm, which allowed use of the UV-Vis spectroscopy method. The rejection value of the membrane for a given sample was calculated by the following formula;

$$B = 100 \left(1 - \frac{C_p}{C_r} \right) \tag{4}$$

where B is percent of tramp oil rejected by the membrane, C_p is the tramp oil concentration in the permeate, and C_r is the tramp oil concentration in the retentate.

3.3 Tramp Oil Contamination Experiment Results

Figures 27-30 show the flux results of the tramp oil contamination experiments. Included in the figures are the results of the tramp oil rejection measurements. Figure 27 provides the results of the control experiment of uncontaminated commercial MWF. This allows for flux comparison with the contaminated samples.
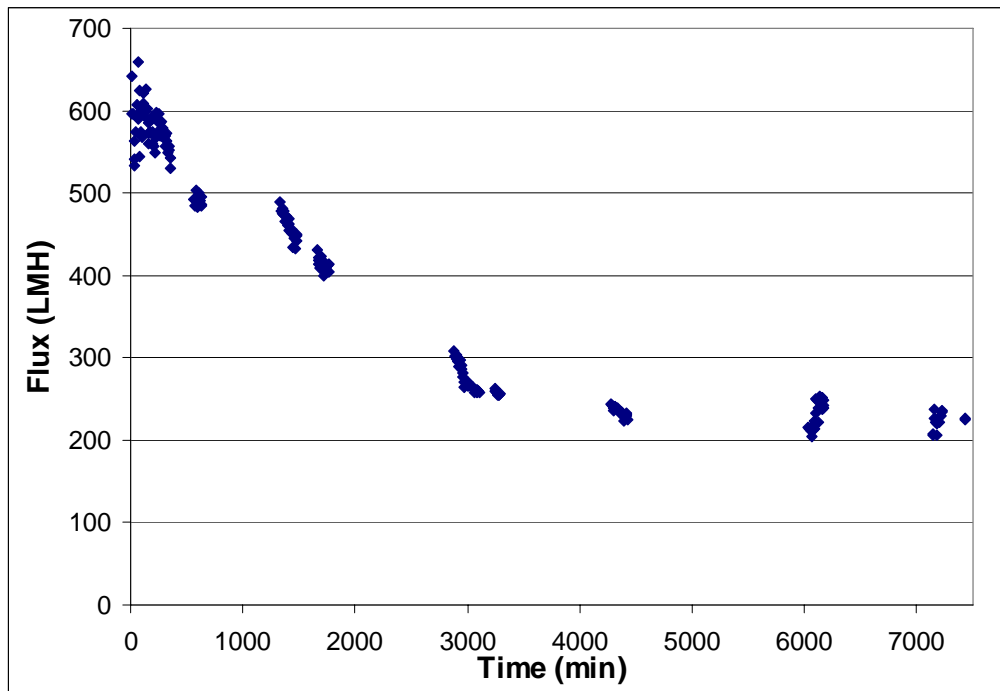
Figure 27 – Uncontaminated Semi-Synthetic MWF Flux

Figure 28 shows the flux behavior and tramp oil rejection of a concentration of hydraulic oil that is increased from 1% to 3% during the test. Figure 29 shows the flux behavior and tramp oil rejection of a new membrane as the hydraulic oil concentration is increased from 1% to 5% over the time of the test. Figure 30 shows the flux behavior and tramp oil rejection of a concentration of hydraulic oil that is increased from 1% to 2% during the

test coupled with a concentration of way oil that is increased from 0.5% to 1% during the test. The results for all of the tests are also provided in Table 8.

Table 8 – Tramp Oil Contamination Results

Test No.	Prior CWF	Intitial Flux	Steady-State Flux	High Rejection (time)	Low Rejection (time)
1	767 LMH	382 LMH	175 LMH	100% (75 min)	98.92% (4635 min)
2	640 LMH	570 LMH	186 LMH	99.99% (80 min)	96.29% (4440 min)
3	760 LMH	380 LMH	226 LMH	99.73% (2940 min)	99.36% (2820 min)
4	758 LMH	641 LMH	234 LMH	NA	NA
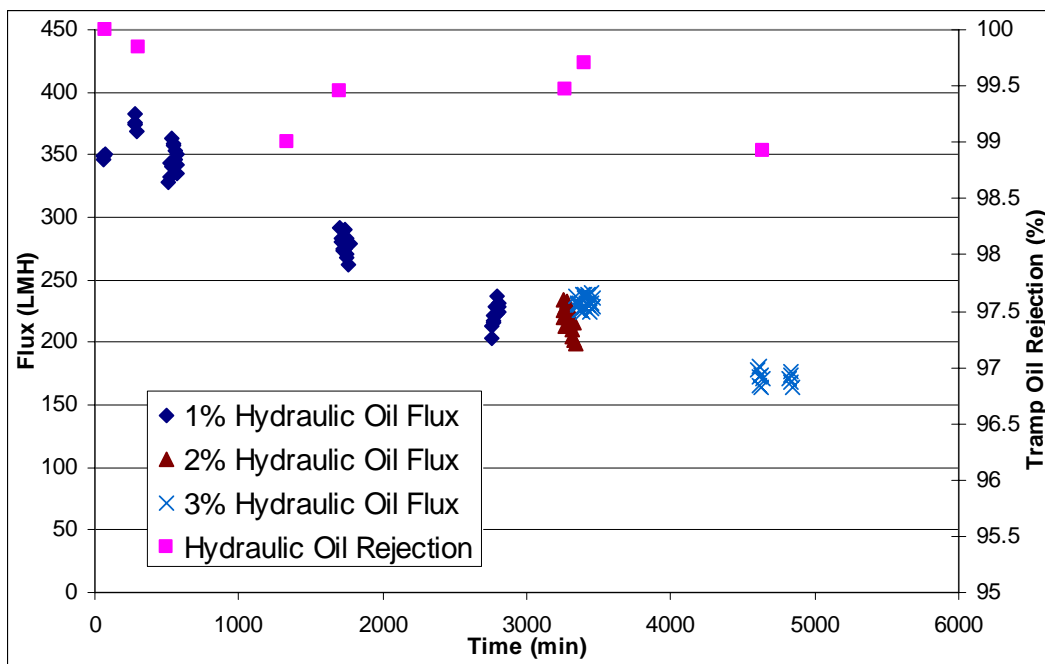
Figure 28 – 1%-3% Concentration of Hydraulic Oil
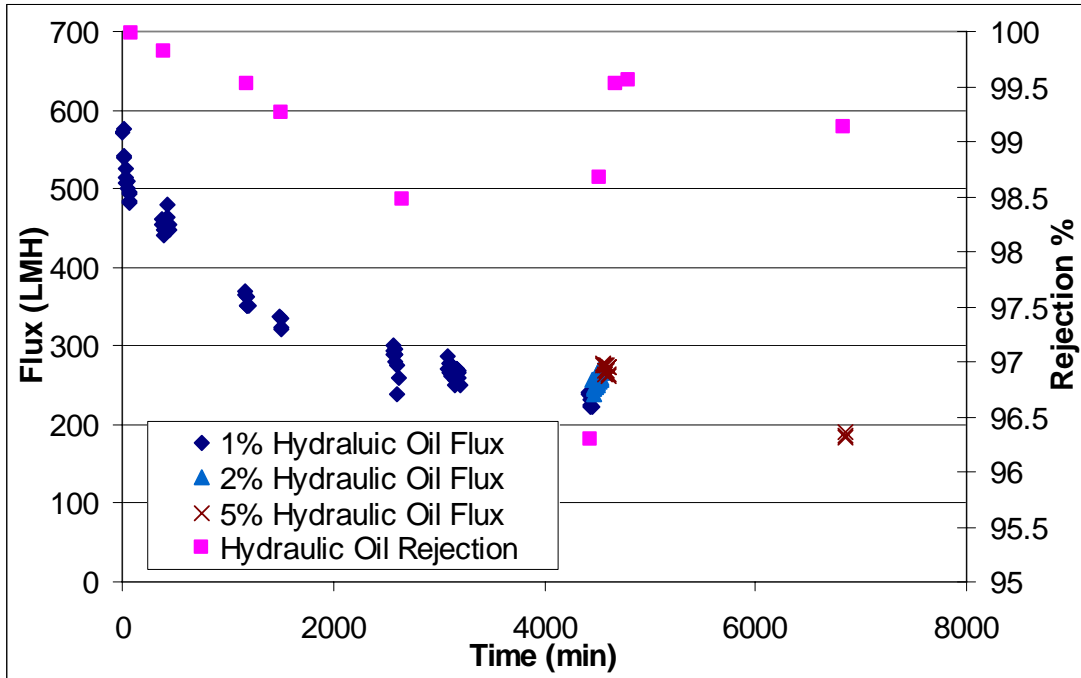
Figure 29 – 1%-5% Concentration of Hydraulic Oil
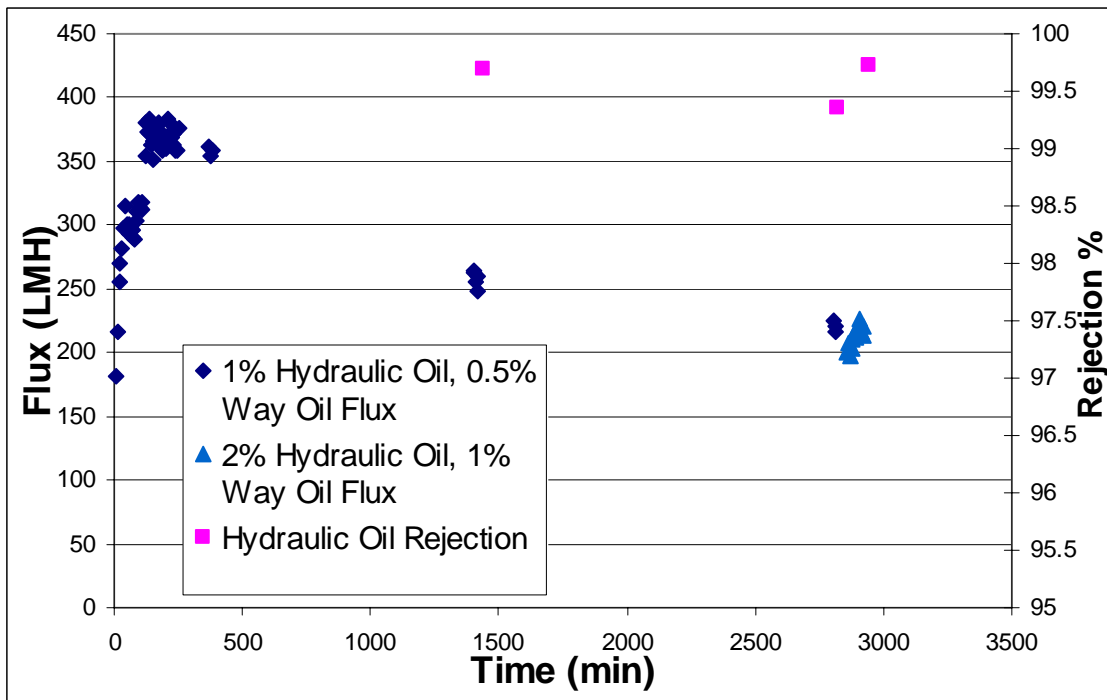
Figure 30 – 1%-2% Hydraulic Oil and 0.5%-1% Way Oil

55

3.4 Discussion of Contaminated MWF Microfiltration Experiments

Table 8 shows, that the final flux level reached by the microfiltration system is between 175 and 250 LMH, regardless of the level of tramp oil contamination. It also appears that the concentration of tramp oil does not seem to affect the system flux. This is indicative of a gel/cake layer being the predominant fouling mechanism within the system. In such a case, the cake layer is built up and the thickness of this layer determines the flux of the membrane. The thickness of the cake layer is determined by operational parameters such as cross-flow velocity and transmembrane pressure as mentioned in Section 3 of this report.

It is important to note that the rejection property of the membranes is strong throughout the tests. At no point does the rejection fall below 96% and, with the exception of two samples, the rejection is consistently above 98.5%. This relates to average tramp oil concentrations in the system permeate of 136 ppm compared to between 10,000 and 50,000 ppm in the feed. The concentration of tramp oil in the feed did not show a correlation to the tramp oil rejection. There was a correlation between filtration time and tramp oil rejection in the initial stages of the test, before steady-state flux was reached. This can be explained by the mechanism by which hydraulic oil emulsions pass through the membrane pores that are smaller than the oil droplets themselves. Some larger pores are coated by the hydraulic oil. The deformable nature of the emulsions allows them to slide through as shown on the right in Figure 31. The kinetics of the coating process is what keeps the rejection level around 100% for the first part of the tests.
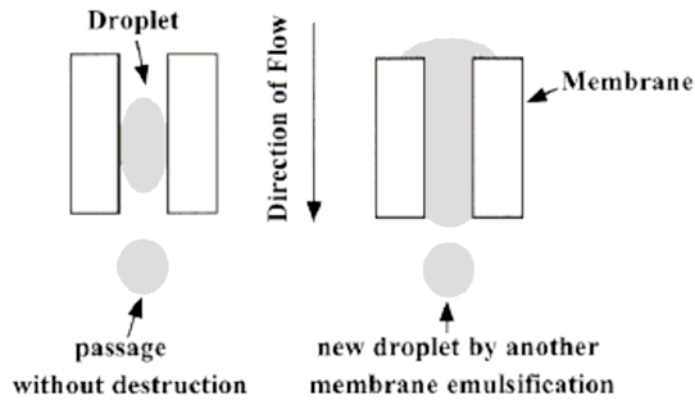
Figure 31 – Transmission of deformable emulsions through membrane [20]

3.5 Summary of Microfiltration of MWF with Tramp Oil Contamination

It was found that 0.5 μm pore size α-alumina membranes were able to reject tramp oil contamination at rates in excess of 96%. The final steady-state membrane flux was not found to be significantly impacted by the presence of tramp oils, including concentrations as high as 5% of hydraulic oil in the feed stream. Two types of tramp oils were tested for effect on membrane performance. It was found that both hydraulic oil and a blend of hydraulic oil and way oil performed similarly.

4. DEVELOPMENT OF A SEMI-SYNTHETIC MWF FOR USE WITH MICROFILTRATION

The majority of membrane anti-fouling research has focused on mechanical methods to fight fouling [21]. These methods include backpulsing, baffles and membrane surface modification [21,22]. In addition, much work has been done on selecting the proper operating conditions to reduce fouling [23]. However, these methods only serve to slow fouling, rather than reduce or eliminate it. The research presented in this section focuses on the design of a semi-synthetic MWF that reduces the fouling phenomenon when used with microfiltration, based on the principles of component adsorption and repulsive interparticle electrostatic interactions.

4.1 Fluid Development

4.1.1 Theoretical Basis

Membrane fouling by semi-synthetic MWFs has been shown experimentally to be caused by three mechanisms: (1) pore constriction due to component adsorption; (2) formation of micro-emulsion aggregates that block pores; and (3) pore constriction due to micro-emulsion deposition on the membrane surface [24, 25].

Component Adsorption

Component adsorption contributes to membrane fouling in two ways: physical pore radius reduction; and the drag force exerted by the extension of the 'brushes' of adsorbed surfactant molecules [26]. The extent to which a surfactant molecule, such as the emulsifiers used in semi-synthetic MWFs, adsorb to membrane surfaces is dependent on

the relative chemistries of the component and surface. Several surfactant molecules have been shown to adsorb strongly to the α-alumina material used as membranes in this research [27-29]. Therefore, it is important to test the emulsifiers used in the semi-synthetic MWF formulation to determine their proclivity to adsorb onto the membranes.

Aggregate Formation and Particle Deposition

Aggregates of micro-emulsions are formed when the inertial momentum of a particle overcomes the electrostatic repulsive force between particles that rises from the electrostatic double layer of each particle. Once the particle overcomes this repulsive force, it is captured due to the attractive van der Waals force present at such short distances. In order to engineer a semi-synthetic MWF that minimizes formation of these aggregates, the repulsive force should be increased to a level where the inertial force seen by the particles is overcome by the electrostatic double layer force.

The Verwey and Overbeek electrostatic double layer equation for identical particles carrying identical surface potentials in a dielectric fluid [30] is given as:

$$W_{dl} = 2\pi R \varepsilon \varepsilon_0 \psi_0^2 e^{-\kappa D} \tag{5}$$

where W_{dl} is the interaction energy between the particles; R is the radius of the particles; ε is the dielectric constant of the medium; ε_0 is the permittivity of free space; ψ_p is the surface potential of the particles; κ is the inverse Debye length; and D is the separation between the particles. The electrostatic repulsive force between the two particles is found by taking the partial derivative of the electrostatic energy with respect to the separation distance:

$$F_{dl}(D) = \frac{\partial W_{dl}(D)}{\partial D} = -2\pi R \varepsilon \varepsilon_0 \kappa \psi_p^2 e^{-\kappa D} \qquad (6)$$

with the negative sign indicating repulsion.

Deposition of MWF micro-emulsions on the surface of the membrane is similar to the process described for aggregate formation. The inertial energy of the particle must overcome the electrostatic repulsive energy between the particle and the membrane surface prior to being captured by van der Waals forces. The equation governing this case:

$$F_E = 2\pi\kappa\varepsilon\varepsilon_0 \left[\frac{2\psi_p\psi_m \exp(\kappa D) - (\psi_p^2 + \psi_m^2)}{\exp(2\kappa D) - 1} \right], \qquad (7)$$

is very similar to Equation (6) with ψ_p being the particle surface potential and ψ_m being the membrane surface potential. The α-alumina membranes are negatively charged, thus the micro-emulsions should also carry a negative charge to incorporate the electrostatic repulsive force between the membrane and the particles in fouling reduction.

From Equations (6) and (7), it can be seen that four parameters can be adjusted in MWF formulations to decrease aggregate build-up and reduce fouling. These four parameters are: particle size, dielectric constant, inverse Debye length, and surface potential. The MWF solutions are more than 95% water so, regardless of the emulsifier package used, the dielectric constant will remain relatively constant. The inverse Debye length, κ, is calculated by:

$$\kappa = \sqrt{\frac{\sum_i \rho_{\infty i} e^2 z_i^2}{\varepsilon\varepsilon_0 kT}}, \qquad (8)$$

where ρ_∞ is the concentration of a given ion; e is the charge on an electron; z is the number of charges on an ion (e.g. 2 for Ca^{2+}); k is the Boltzmann constant; T is the absolute temperature; and the other nomenclature is the same as in Equation (5).

From Equation (8), it can be seen that the inverse Debye length is proportional to the square root of the ionic strength on the medium. Therefore, in order to decrease the interaction energy within the MWF, the ionic strength of the solution must be lowered, an unrealistic option. This leaves the particle size and the surface potential of the particles as the adjustable parameters.

According to Equation (6), the interparticle repulsive force is proportional to the radius of the particles. Therefore, it would be natural to increase the particle size in order to increase the repulsive force. However, the process of microfiltration of semi-synthetic MWFs is dependent on the micro-emulsion being as small as possible. This is due to the selective separation nature of the process, which requires the native MWF micro-emulsions to be small enough to pass easily through membrane pores that would catch larger emulsions formed from contaminating tramp oils. Due to this dependence on the small size of the micro-emulsions, it is not an option to increase the interaction energy by increasing the particle size. This leaves the surface potential of the particles as the only choice for adjustment.

The electrostatic repulsion force is proportional to the square of the surface potential, making it the variable that can most efficiently cause change in the repulsive force. This

is also the easiest parameter to adjust because it depends totally on the choice of the anionic surfactants, non-ionic surfactants and couplers that make up the emulsifier package. Thus, this research focuses on designing a non-fouling semi-synthetic MWF by adjusting this variable.

4.1.2 Fluid Composition

Semi-synthetic MWF components can be broken down into three groups: aqueous components, oil soluble components, and emulsifiers. The oil phase is generally used as the lubricating agent, the aqueous phase is used for cooling, and the emulsifiers are used to maintain the phase separation necessary to keep the suspension dispersed. Semi-synthetics are typically produced in concentrated form with oil as the continuous phase. These concentrated fluids are then diluted to a 5-10% concentration in water prior to use.

Approximately 50% of semi-synthetic metalworking fluid concentrate volume consists of the aqueous phase. Biocides and defoamers can both be present in the aqueous phase. The oil phase in a diluted fluid is contained within micro-emulsions generally between 0.1 and 0.01 μm in diameter. The oil soluble components generally consist of a napthenic oil and specialty additives for lubricity and pressure. The emulsifier package used to create the micro-emulsions is typically made up of a combination of alkanolamides, sulfonate bases, soaps, and esters [Byers]. Frequently MWF manufacturers will keep the emulsifier package proprietary because it is the element that most differentiates between semi-synthetic MWFs. The choice of emulsifiers determines the stability and clarity of the fluid by regulating the size and surface potential of the

emulsions. The general formulation of the commercial semi-synthetic MWF used in the research reported in previous sections of this report and used in this section for comparison purposes is provided in Table 9.

Table 9 – Commercial Semi-Synthetic Concentrate Formulation

Function	Component	% by wt.
Oil	Napthenic	30-35
Emulsifier	Sulfonate Base	1-5
Emulsifier	Non-ionic (proprietary)	5-10
Corrosion inhibitor	Boric acid	1-5
Biocide/Fungicide	Triazine/pyridiethione	1-2
Diluent	Water	40-60

In this research, five commonly used semi-synthetic MWF components are investigated: napthenic oil; sodium sulfonate; an alkanolamide; oxazoline; and ethylene glycol monobutyl ether (EB). If MWF components already being used in MWF production are shown to be conducive for use with microfiltration then it will be a relatively straightforward adjustment for manufacturers to start producing microfiltration compatible semi-synthetic MWFs. No biocide was used in the formulation of the semi-synthetic due to the fact that it is specifically designed to be used with microfiltration. The microfiltration process itself removes harmful bacteria and renders the inclusion of a biocide additive unnecessary.

Napthenic oil was chosen because most lubricant additives are more soluble and compatible in napthenic oils than in paraffinic or vegetable oils [31]. The napthenic oil forms the base of the oil phase. In field applications, the oil content of semi-synthetic

fluids is generally kept at a constant level for a given machining operation in order to maintain the lubricity component [25].   Therefore, even though previous research has shown that reducing oil content leads to higher flux, because it lessens pore blocking and pore constriction [25], the oil level in the designed fluid will be kept at the same level as in the commercial fluid (approximately 30%).

Petroleum-based sodium sulfonate is a two-tailed amphiphilic molecule with the polar head consisting of a SO_3^- Na^+ species and each hydrophobic tail consisting of a C_{15} to C_{30} alkyl chain. This anionic surfactant was chosen as the primary emulsifier because of its use in a large number of commercial semi-synthetic MWFs. It is also known to have a relatively high negative charge when dispersed in water.

Most semi-synthetic MWF formulations use a combination of anionic and non-ionic surfactants to emulsify the oil phase. A 2:1 tall oil fatty acid alkanolamide was chosen as the non-ionic surfactant for the designed fluid due to its ability to create small micro-emulsions.   The specific additive used (Actramide 202, DOW) is advertised as also providing some measure of the desirable characteristics of low foaming, good lubricity and corrosion protection.

MWF concentrates are typically formulated so that upon dilution they will provide alkaline solutions. The proper degree of alkalinity maximizes the fluid properties of corrosion inhibition, emulsion stability, solution clarity, and lubricity [32].   An ethozylated oxazoline derivative (Alkaterge IV, ANGUS) was chosen for use as both an

acid scavenger and corrosion inhibitor. The additive was also chosen because it can also be used as a secondary emulsifier and auxiliary coupler, which induces greater clarity and smaller emulsion size in the dilution.

The final component that was investigated was ethylene glycol monobutyl ether (EB). EB is used as an auxiliary emulsifier and mutual solvent in semi-synthetic MWFs. It was chosen for its complete water solubility and high coupling efficiency. The affinity for water indicates a smaller likelihood to adsorb onto the alumina membrane.

The design of the fluid was accomplished by a build-up of the individual components until the complete formulation was reached. The fluid build-up started with just the surfactants and surfactant combinations without oil present. This was done to test the adsorption tendencies of the emulsifiers. Table 10 provides the composition of each fluid created as a concentrate. The concentrated fluids were then diluted to a 5% concentration prior to testing to enable comparison with the diluted commercial fluid. The composition of the final designed fluid (Fluid 6 in Table 10) was determined by matching up components that performed well in fouling tests and combining them into a complete fluid formulation.

Table 10 – Composition of Experimental Fluids

Component	Percentage By Volume In Test Fluid Concentrate					
	Fluid 1	Fluid 2	Fluid 3	Fluid 4	Fluid 5	Fluid 6
Napthenic oil	0.00%	0.00%	0.00%	0.00%	30.00%	30.00%
Sodium sulfonate	22.00%	22.00%	22.00%	22.00%	22.00%	22.00%
Fatty acid alkanolamide	0.00%	5.00%	0.00%	5.00%	5.00%	5.00%
Oxazoline	0.00%	0.00%	6.00%	6.00%	6.00%	6.00%
Ethylene gylcol monobutyl ether	0.00%	0.00%	0.00%	0.00%	0.00%	3.00%
DI Water	78.00%	73.00%	72.00%	67.00%	37.00%	33.00%

In order to eliminate any variance due to pH change in tests between the designed fluids and the commercial fluid, the fluids were titrated with a 1% solution of 2-amino-2-methyl-1-propanol until the pH was constant. The concentrations of each fluid shown in Table 10 were chosen because they were close to the values given in Table 9 for the commercial fluid, which was used for comparison purposes.

Some combinations of emulsifiers were unstable and caused precipitates to form, which is undesirable. Table 11 shows the results of the mixing of each fluid. Fluids 2 and 4 formed a light-colored, fluffy precipitate on the bottom of the beaker after sitting for 24 hours. However, all of the other fluids formed highly stable dispersions that did not separate out over the span of six months. Fluids 1 and 3 both formed clear fluids that were yellowish in color. Fluids 5 and 6 were both tan in color and slightly opaque.

Recall that two major considerations in membrane fouling by metalworking fluids are the size of the micro-emulsion and its surface potential. The strength of the charge on the emulsions is also the primary factor in the stability of the suspension. The particle sizes, pH at 20°C, and ξ-potential of each fluid are provided in Table 12. Particle sizes were

determined using photon correlation spectroscopy and ξ-potential values were determined using laser droplet electrophoresis. Both measurement techniques provide a distribution of particle property values gathered from multiple measurements. The values provided in Table 12 for particle size are mean volume values analyzed using the CONTIN model and for ξ-potential are mean values of the measured intensity distributions. Most fluids provided a single peak for both measurements. However, Fluid 5, which contained the emulsifiers plus napthenic oil, gave a very spread out ξ-potential with three peaks of similar amplitudes. Therefore, in order to provide an accurate representation of the distribution, all three peaks are included, rather than a single mean value. The addition of EB was used to provide a smaller emulsion size and less variation in the distribution of the fluid's ξ-potential. There is no data provided for Fluid 4 because phase separation made it unusable. Particle size data for Fluid 2 is not provided for the same reason. Data is provided for the commercial fluid for comparative purposes. Further ξ-potential and particle size data for the fluids are provided in Appendix E.

Table 12 – Particle Size, pH, and ξ-potential Data

Fluid	Zeta Potential (mV)	Particle Size (nm)	pH
1	-92.2	13.2	7.78
2	-111.5	-	8.74
3	-76.9	132.8	9.17
4	-	-	-
5	-115.9, -99.8, -73.7	25.6	9.3
6	-71	21.1	9.36
Commercial	-64	32	9.3

Adsorption tests were carried out to determine the compatibility of components with α-alumina membranes. The ability of the components to interact with the membrane

without pore constriction caused by adsorption provides further evidence that the components are safe to use in MWFs that will be recycled through microfiltration. Fluids 1-6 from Table 2 were tested to determine the extent of pore constriction caused by adsorption of the MWF components. The tests consisted of placing a portion of α-alumina membrane in a beaker containing 150 ml of test fluid and leaving it for 12 hrs. The α-alumina pieces were then dried to 80°C and examined by SEM to look for evidence of adsorption. Adsorption that would adversely impact microfiltration was determined by comparing pore size and sharpness of alumina grain geometry before and after exposure to the fluid. A similar test method had been used previously with the commercial MWF and significant adsorption was visible through the SEM images. SEM images from these previous experiments are shown in Appendix B.

The four membrane pieces that were placed in the fluids were compared to a control piece from the same original membrane. In all cases, the membrane surfaces were identical to the control membrane. From this, it was concluded that none of the MWF components from Table 10 adsorb to α-alumina membranes to an extent that would constrict pores enough to cause a significant negative impact on performance. SEM images of each membrane piece tested are provided in Appendix B.

As can be seen in Table 12, the particle size of the sulfonate and oxazoline formulation (Fluid 3) is significantly larger than the particle sizes of the formulations that include oil (Fluids 5 and 6). This is due to the change in emulsifier behavior in the presence or absence of oil, which can cause much larger particles to be formed. This change in

component behavior means that tests of the fouling and machining performance capabilities of emulsifiers without oil will not provide an accurate measure of the fouling nature of the component in the presence of oil. Therefore, in the remainder of this chapter, only the two semi-synthetic formulations that include oil (Fluids 5 and 6) are compared to the commercial fluid.

4.1.3 Microfiltration Tests for Designed Semi-Synthetic Fluids

The membranes used in the microfiltration tests of the designed fluids were the same type of membranes as previously discussed in Section 2.1. The tubular membranes were cleaned prior to use through the pyrolysis cleaning technique described in 2.1. The disk membranes used for SEM imaging were new from the manufacturer and were therefore assumed clean. The same microfiltration setups were used as described in the experiments of Section 2.1. The tubular membrane tests were conducted with a cross-flow velocity of 6 m/s and a transmembrane pressure of 0.255 bar. Tests on the disk membrane system were conducted at a cross-flow velocity of 3.3 m/s and a transmembrane pressure of 0.255 bar. The geometries of the two systems made it impossible to maintain both the cross-flow velocity and transmembrane pressure constant between the systems. The transmembrane pressure was chosen to be maintained at the same level between the systems due to its importance in the membrane fouling mechanisms as indicated in Section 2. Therefore, it was necessary to use different cross-flow velocities for the systems. System permeate flux was measured by collecting the permeate in a beaker on a balance and recording it with the use of an automated data

collection system. Permeate and retentate samples were taken during each test for refractive index analysis.

Fouling tests were conducted using the designed semi-synthetic MWF formulations (Fluids 5 and 6) and compared to the results from Section 2 for the commercial semi-synthetic fluid. The tests were run at a 5% concentration of the fluids developed in Table 10 with the balance being made up of water purified to 18MΩ resistivity to eliminate fouling due to contaminants in the water. Each fouling test lasted until the flux through the membrane reached a steady-state value, therefore the filtration time varied between fluids.

4.2 Results of Fouling Experiments for Designed Fluid

Membrane fouling was judged through four criteria: (1) the final steady-state system flux; (2) the time the system takes to reach steady-state; (3) the fluid transmission as indicated by refractive index; and (4) SEM images of membrane surfaces following fouling tests. For the three test fluids, data for all but the fourth criteria are given in Table 13 along with the water flux and initial flux for each fluid. The fluid transmission column of Table 13 indicates the percent of MWF components that pass through the membrane without being rejected as indicated by refractive index measurement.

Table 13 – Fouling Tests for Designed Fluids

Fluid	Water Flux (LMH)	Initial MWF Flux (LMH)	Steady-State Flux (LMH)	Time to Steady State (min)	Fluid Transmission at Steady-State (%)
5	650	316	480	250	100
6	919	452	500	80	100
Commercial	758	600	220	4400	90

Figures 32, 33, and 34 illustrate the flux behavior of the three fluids from Table 13. A significant difference can be seen between the flux curve of the commercial fluid (Figure 32) and the flux curves of the designed fluids (Figures 33 and 34). The flux of the designed fluids stays constant at a single flux value throughout the testing rather than showing the flux decrease evidenced in Figure 32 for the commercial fluid. Note that Figure 32 divides the flux curve into two portions (A and B), as previously seen in Section 2.2. This division provides a distinction in membrane fouling behavior discussed below.
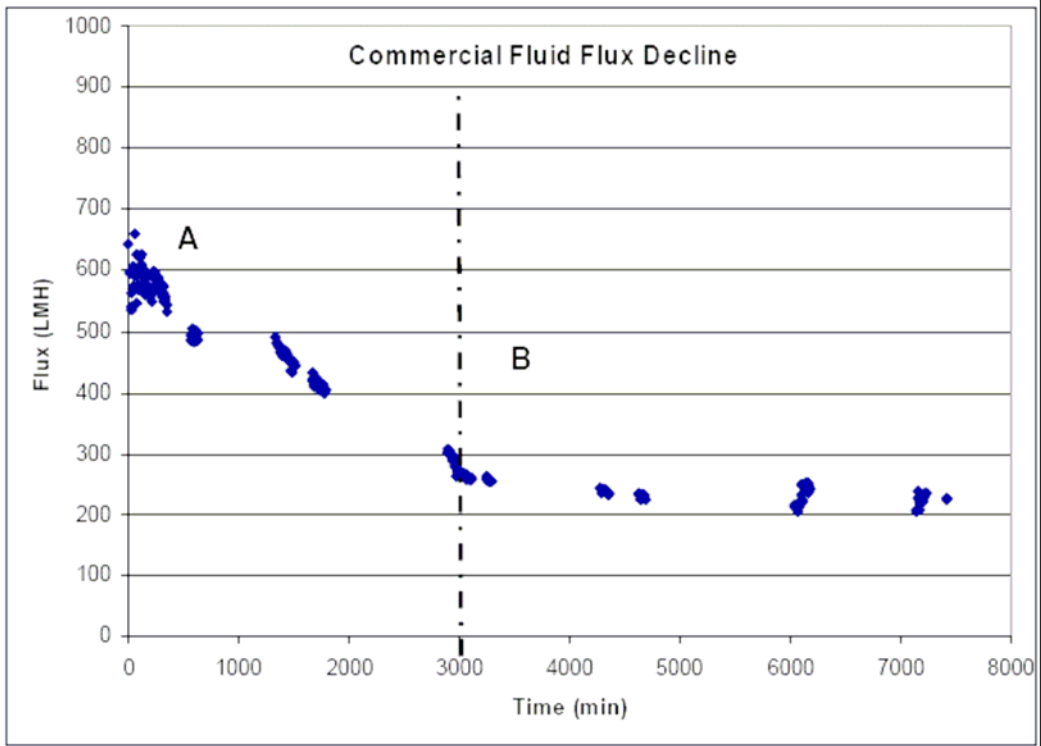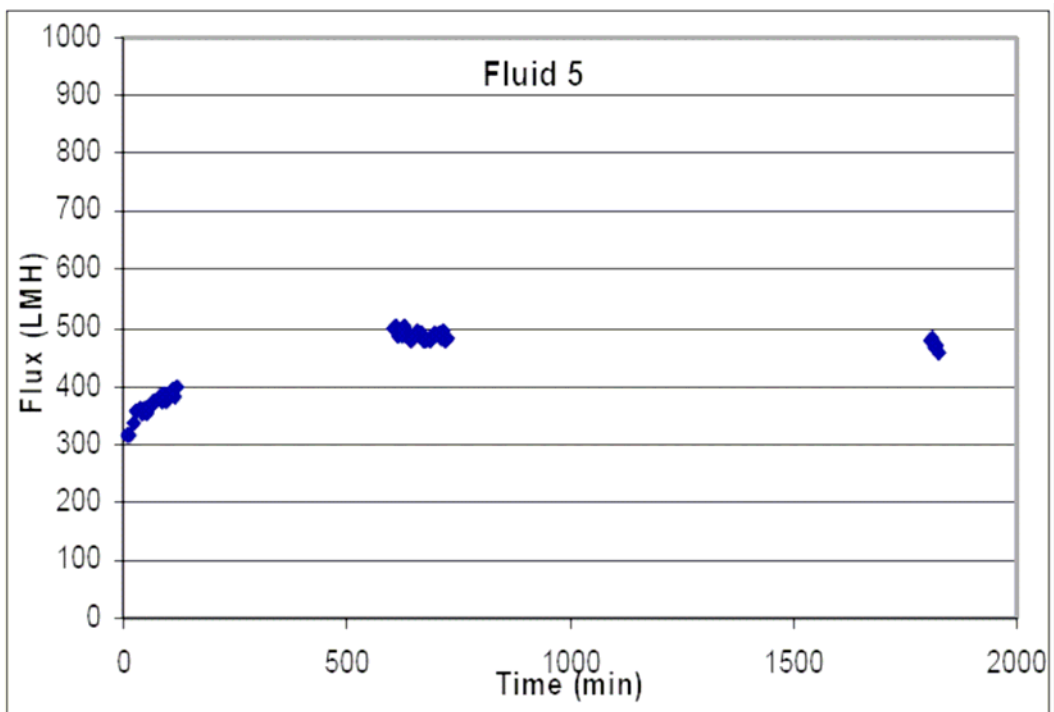
Figure 32 – Commercial Fluid Flux Decline

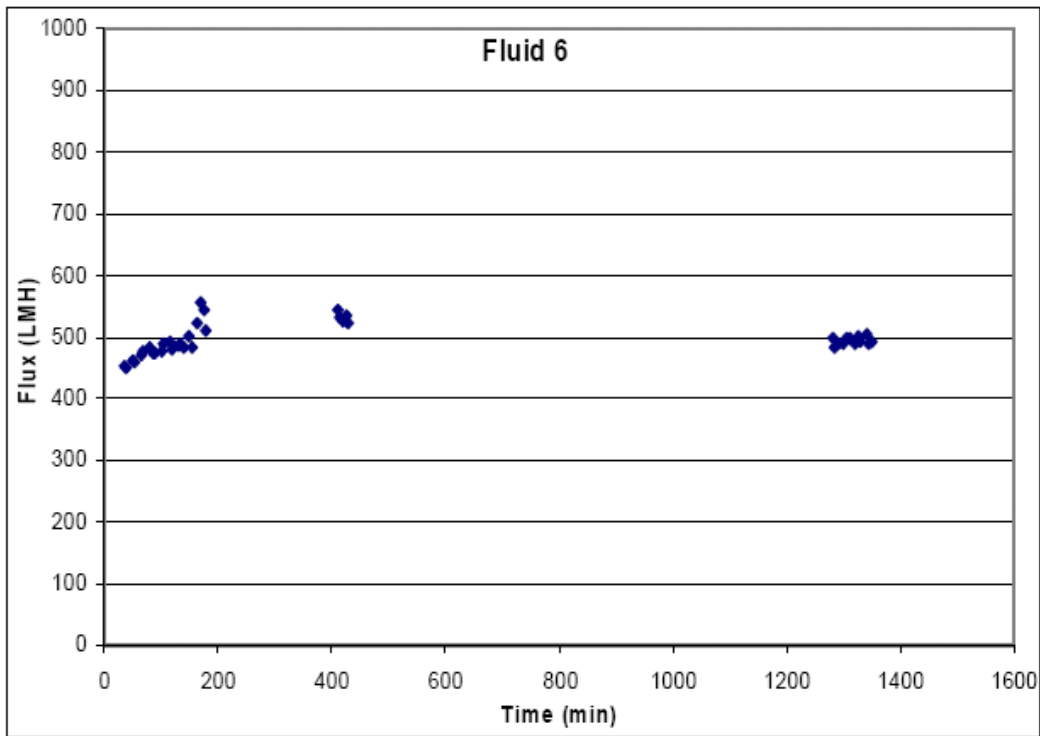
Figure 33 – Flux Behavior of Fluid 5

Figure 34 – Flux Behavior of Fluid 6

4.3 Discussion of Microfiltration Test Results for Designed Fluids

The flux curve of the commercial fluid in Figure 32 shows a sharp linear decrease for the first 3000 minutes, followed by a less steep linear decrease until steady-state is reached at 4500 minutes. As discussed in Section 2.3, the curve is broken into two sections (A, B) that indicate the predominant fouling mechanism present. Section A indicates particle deposition on the membrane surface and the resulting pore constriction. Section B is representative of the formation of the particle cake layer on the membrane surface. It is hypothesized that the significant amount of time necessary for the commercial fluid to reach steady-state is due to the formation of the cake layer. Furthermore, the cake layer is assumed to continue to build-up even after steady-state is reached. However, at steady-

73

state the cake formation is fully countered by the removal of cake build-up from hydrodynamic drag due to the fluid cross-flow.

The flux behavior shown in Figures 33 and 34 of the designed fluids is opposite that of the commercial fluid. Rather than decreasing, the flux initially increases. The fluid flux then remains at a constant rate for the duration of the test. This flux behavior is ideal for microfiltration processes because it allows for a constant flux rate to be used in flow calculations. When a continually changing flux causes membrane fouling, it becomes difficult to maintain the flow volumes needed by each machining tool using MWF. In addition to not showing evidence of membrane fouling, the proposed fluid has a steady-state flux (500 LMH) more than twice that of the commercial fluid (220 LMH).

In order to understand the difference in fouling behavior between the commercial and designed MWFs, it is necessary to understand the differences in certain key properties of the fluids. The particle size and ξ-potential data (Table 12) for the designed fluids are both smaller and significantly more negatively-charged than the commercial fluid. The α-alumina membranes carry a negative charge so the negative MWF micro-emulsion particles and membrane experience electrostatic repulsion. As the particles become more negative, these repulsive forces increase and provide more fouling resistance. In addition, the increased electrostatic repulsion lowers fouling due to aggregate blocking and hydrodynamic bridging, i.e., fouling due to more than one particle reaching the pore simultaneously and becoming lodged together at the pore mouth [33].

Further investigation of the membrane fouling of the designed fluids and the commercial fluid were accomplished by SEM imaging. Figure 35 shows a SEM image of a new membrane that has never been exposed to MWF under 20,000X magnification. The spherical objects that make up the structure are the alumina particles that provide the membrane surface. Figures 36 and 37 illustrate the fouling that occurs in the microfiltration of the commercial semi-synthetic fluid. The images show the MWF particle aggregates lying on top of the membrane surface causes the formation of the fouling network. The effect of the interaction between the designed MWFs and the membrane once steady-state has been reached is illustrated in Figures 38 and 39. Further SEM images of the membranes in their various states are provided in Appendix B. The lack of membrane fouling in these figures is clearly evident. In fact, the membranes that have been used to process the designed MWFs and the new membranes are indistinguishable.
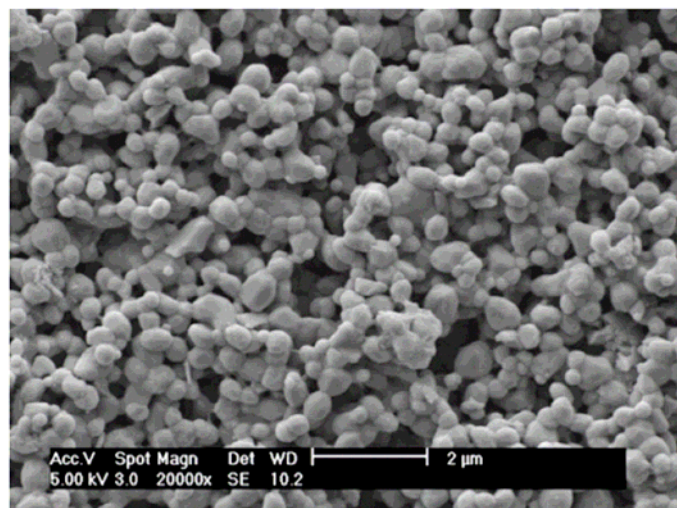

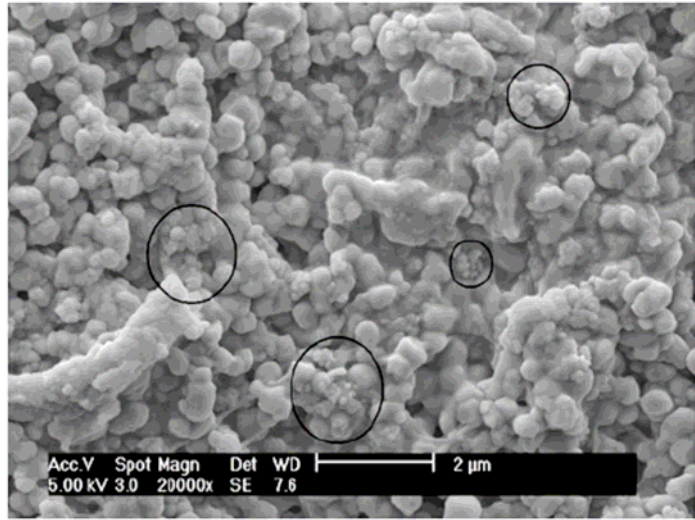Figure 35 – SEM Image of New Membrane (20000X Mag.)

Figure 36 – SEM Image of Membrane Used with Commercial Fluid (Fouling Section A –
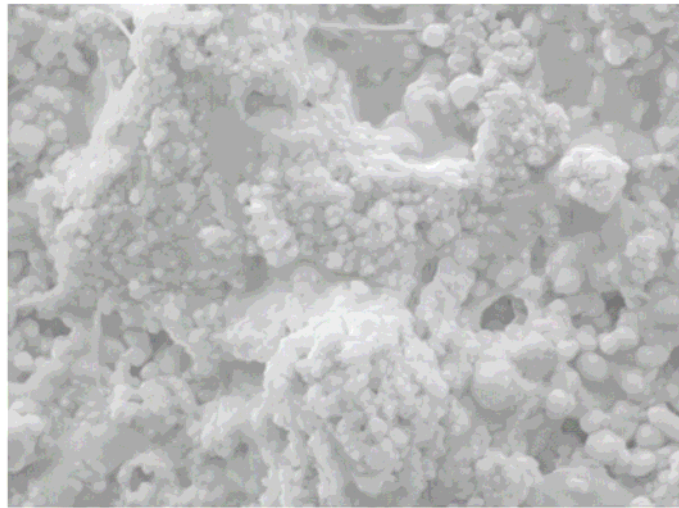
20000X Mag.)

Figure 37 – SEM Image of Membrane Used With Commercial Fluid (Fouling Section B
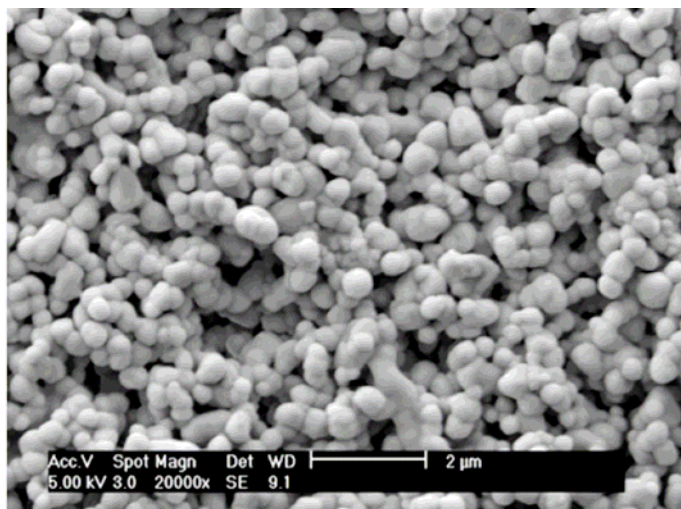
– 20000X Mag.)

Figure 38 – SEM Image of Membrane Used With Test Fluid 5 (20000X Mag.)

Figure 39 – SEM Image of Membrane Used With Test Fluid 6 (20000X Mag.)
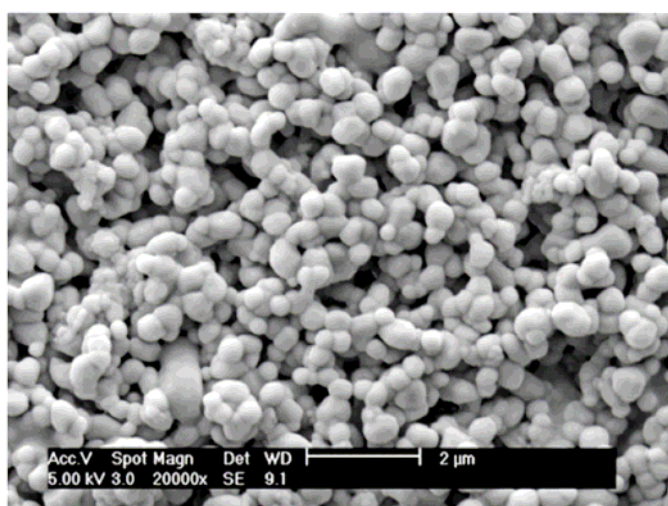
The data provided by the microfiltration fouling tests show that there is no appreciable difference between the microfiltration performance of Fluid 5 (full formulation without EB) and Fluid 6 (full formulation with EB). However, particle size and ζ-potential data provided in Table 12 indicate that the inclusion of EB allows a more uniform ζ-potential

distribution as well as a smaller micro-emulsion size. For this reason, the final semi-synthetic MWF formulation will include EB.

4.4 Cooling and Lubricity Properties of Designed Fluid

4.4.1 Experimental Setup

Tests were performed to examine the lubrication and cooling capabilities of the designed fluid and compare them with test results for the commercial semi-synthetic MWF. Two evaluation test methods were used. A drilling testbed first described by Greeley et al. [16] was used to evaluate drilling torque, thrust, and cutting interface temperature. A schematic of this drilling testbed is given in Figure 40. A tapping torque method developed by Rusk et al. [15] was used to further confirm the lubricity efficacy of the fluids and validate the drilling testbed.
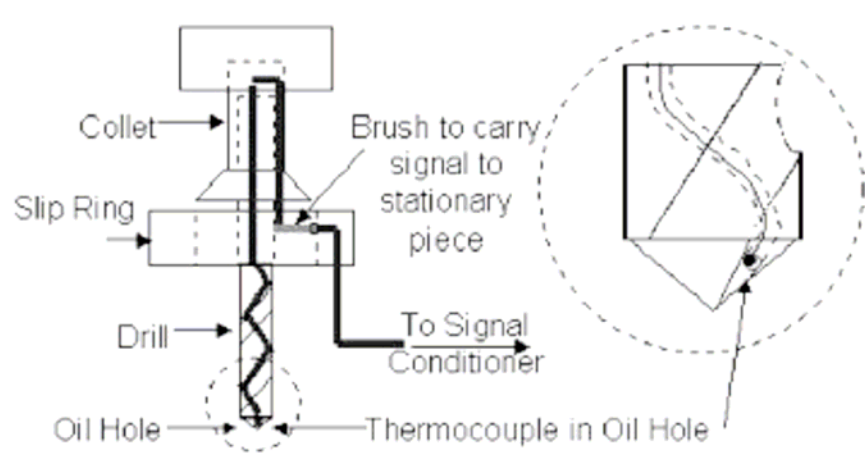

Figure 40 – Schematic of Drilling Testbed [16]

The drill used in the drilling test-bed was a 12.7 mm diameter HSS oil-hole drill with 118° point angle, 33° helix angle, a notched point, and a 1.07 mm chisel edge. The

thermocouple that records interface temperature data resides in the oil hole just behind the cutting edge.

The workpiece used in the experiments was made out of 1018 steel. Each drilling test was carried out using a 3.175 mm diameter pilot hole to eliminate indentation/extrusion effects of the chisel edge thus allowing acquisition of temperature and forces that were generated only along the drill's cutting edge. MWF-based drilling conditions were accomplished by pre-counterbored workpieces that allow a pool of MWF to surround the drill when cutting. In order to remove oils and contaminants between test trials, the drill and workpiece were both rinsed with acetone.

The drill was operated at a cutting speed of 30.32 m/min with a federate of 135 mm/min during testing. The holes drilled in each test were 12.7 mm deep. The torque and thrust data used in the results and analysis from these experiments are the average of the cutting forces during the time that the drill was fully engaged in the workpiece. Temperature data taken from the thermocouple is recorded as the maximum observed temperature during the drilling cycle. Figure 41 shows typical data collected during a test and the portion of the data used as the response.
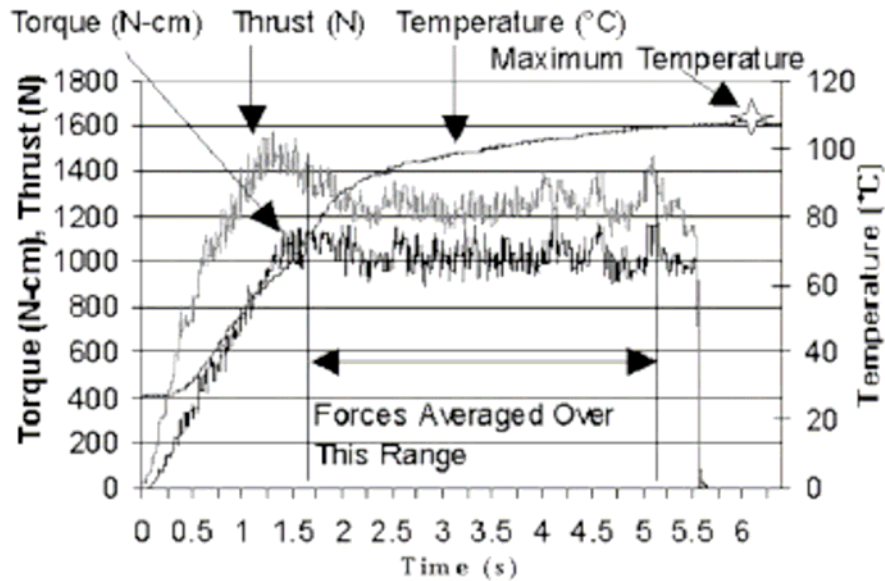
Figure 41 – Typical Drilling Test-bed Response [16]

The tapping torque test was based on ASTM Standard D5619-00(2005). A M8x1.25 tap was used in a bench-top tapping machine on 1018 steel workpieces. The final torque value given for each test in the results and used in the statistical analysis of the tests is the average of the torque values recorded while the tap was fully engaged in the workpiece.

4.4.2 Analysis of Cooling and Lubricity Test Results

Cooling and lubricity tests were conducted for three fluids in order to compare them. These three fluids were a 5% concentration of the commercial semi-synthetic MWF, a 5% concentration of Fluid 6, and DI water. The test for each fluid consisted of six (6) replicates on the drilling test-bed and nine (9) replicates on the tapping-torque machine. The tests were run in a randomized order within each method. The results for the drilling test are given in Table 14. The results for the tapping torque tests are provided in Table 15.

Table 14 – Drilling Test Results

Fluid	Test 1	Test 2	Test 3	Test 4	Test 5	Test 6	Mean	Std. Dev.
DI H2O								
Average Torque (N-cm)	1130.87	1136.11	1130.73	1099.97	1095.66	1133.53	1121.15	18.23
Average Thrust (N)	1184.25	1195.92	1187.50	1172.60	1188.17	1192.40	1186.80	8.06
Max Temp (°C)	103.34	100.94	99.14	92.54	96.14	100.94	98.84	3.90
Commercial								
Average Torque (N-cm)	1063.12	1084.73	1080.21	1072.12	1098.44	1104.33	1083.83	15.58
Average Thrust (N)	1127.23	1135.74	1133.33	1115.37	1165.28	1159.65	1139.43	19.26
Max Temp (°C)	93.14	90.13	89.53	87.73	86.53	88.33	89.23	2.30
Fluid 6								
Average Torque (N-cm)	1099.80	1096.38	1093.44	1105.93	1084.71	1073.73	1092.33	11.51
Average Thrust (N)	1131.99	1143.79	1154.72	1180.85	1152.76	1148.73	1152.14	16.24
Max Temp (°C)	91.33	91.33	88.93	86.53	87.13	88.93	89.03	2.02

Table 15 – Tapping Torque Results

Fluid	1	2	3	4	5	6	7	8	9	Mean	Std. Dev.
DI H20	298.16	288.06	284.13	284.18	315.25	312.79	307.99	292.16	307.49	298.91	12.32
Commerical	270.35	273.08	268.56	271.94	235.07	276.97	289.78	290.02	294.70	274.50	17.69
Fluid 6	272.01	283.63	281.19	269.50	275.70	278.76	297.59	299.23	300.05	284.18	11.22

The results for both the drilling tests and the tapping torque tests were analyzed for possible differences in performance for all possible pair-wise comparisons of the three fluids for each of the four responses. The statistical significance was evaluated using a student's t-distribution with an α-level of 0.05. Table 16 provides a summary of the results of these tests for statistical significance.

Table 16 – Statistical Results of Fluid Performance

Fluid 1	Fluid 2	Mean Difference	t-value	t-critical	Significant
Drill Torque					
DI H2O	Com.	37.32	3.81	2.262	yes
DI H2O	Fluid 6	28.81	3.27	2.262	yes
Com.	Fluid 6	-8.51	1.08	2.262	no
Drill Thrust					
DI H2O	Com.	47.37	5.56	2.262	yes
DI H2O	Fluid 6	34.66	4.68	2.262	yes
Com.	Fluid 6	-12.71	1.24	2.262	no
Drill Temperature					
DI H2O	Com.	9.61	5.19	2.262	yes
DI H2O	Fluid 6	9.81	5.46	2.262	yes
Com.	Fluid 6	0.20	0.16	2.262	no
Tapping Torque					
DI H2O	Com.	25	3.40	2.12	yes
DI H2O	Fluid 6	15	2.58	2.12	yes
Com.	Fluid 6	10	1.36	2.12	no

The data in Table 16 show that both Fluid 6 and the commercial fluid performed significantly better than DI water in drill torque, drill thrust, drill temperature, and tapping torque. Fluid 6 and the commercial fluid compare well in drill torque, drill thrust, drill temperature, and tapping torque tests, showing no statistical difference. The performance of the designed fluid, in terms of measures of lubricity and cooling, cannot be distinguished from the commercial fluid.

4.5 Designed Semi-Synthetic MWF Summary

In this chapter, the development of a semi-synthetic MWF specifically engineered for use with α-alumina microfiltration membranes was described. It was shown that by understanding the mechanisms that govern membrane fouling, it is possible to design semi-synthetic MWFs that transmit fully through microfiltration membranes without fouling. The following conclusions were reached:

1. A designed semi-synthetic MWF formulation consisting of napthenic oil emulsified by sodium sulfonate, a fatty acid alkanolamide, an oxazoline and ethylene glycol monobutyl ether creates a very strongly electronegative (-71 mV) and very compact emulsion (17 nm) that is stable over long period of time (6 months).

2. During microfiltration tests at low pressure (0.255 bar) and high cross-flow velocity (6 m/s), the designed fluid exhibits a constant microfiltration flux without exhibiting flux decline due to membrane fouling.

3. SEM images show that there is no membrane fouling evident on the surface of membranes used for microfiltration of the designed semi-synthetic MWF.

4. Cooling and lubricity tests show that results for the designed semi-synthetic MWF cannot be distinguished from those of a commercial semi-synthetic MWF, when tested on both a drilling testbed designed for MWF comparisons and a tapping torque machine.

5. CONCLUSIONS

In this research, it was found that microfiltration of semi-synthetic metalworking fluids is a useful technology for reducing contaminants within a MWF stream. The efficiency of this technology was found to be dependent on several system properties, such as operational parameters and membrane and fluid chemistry. By adjusting these properties, the efficacy of the process can be significantly increased.

The fouling mechanisms present in the microfiltration of semi-synthetic MWFs were investigated through microfiltration tests using an uncontaminated commercial fluid in varying concentrations. The effect of the operational parameters of the microfiltration system on membrane fouling was investigated to determine how to attain optimized system performance. The parameters of transmembrane pressure, cross-flow velocity, and backpulsing were varied in microfiltration tests using a membrane that had previously attained steady-state fouling. It was determined that:

1. Within the concentration levels tested, 1%-5%, the concentration of an uncontaminated semi-synthetic MWF does not have an effect on the end flux level reached in microfiltration.

2. For a given set of operating parameters, membrane fouling occurs first by deposition of particle aggregates on the membrane followed by the formation of a cake layer.

3. Fouling caused by the formation of a cake layer can be reversed, to a certain extent, by surfactant washing and changes in operational parameters.

4. Increasing cross-flow velocity within the system can retard the formation of a cake layer.

5. In the presence of a cake layer, flux is responsive to changes in transmembrane pressure only in the presence of backpulsing. In the absence of backpulsing, flux is dependent on cross-flow velocity.

6. Backpulsing is most effective for systems run at high transmembrane pressures.

The ability of the microfiltration membranes to remove tramp oil contaminants was investigated. Two model oils (hydraulic oil and way oil) were added to the commercial MWF and the system was run under optimized conditions. The following conclusions were drawn.

1. α-alumina membranes with 0.5 μm pores were able to reject tramp oil at rates in excess of 96%.

2. The final steady-state membrane flux was found to not be significantly impacted by the presence of tramp oils in the feed stream in concentrations as high as 5% by volume.

A semi-synthetic MWF was specifically developed for use with α-alumina microfiltration membranes. The design of the fluid was based on understanding and combating the membrane fouling mechanisms at work in the microfiltration process. The designed fluid was tested for its ability to be used with microfiltration and also its lubricating and cooling properties. The conclusions reached from this research were:

1. By understanding the mechanisms that govern membrane fouling, it is possible to design semi-synthetic MWFs that transmit fully through microfiltration membranes without fouling.

2. A designed semi-synthetic MWF formulation consisting of napthenic oil emulsified by sodium sulfonate, a fatty acid alkanolamide, an oxazoline and ethylene glycol monobutyl ether creates a very strongly electronegative (-71 mV) and very compact emulsion (17 nm) that is stable over long period of time (6 months).

3. During microfiltration tests at low pressure (0.255 bar) and high cross-flow velocity (6 m/s), the designed fluid exhibits a constant microfiltration flux without exhibiting flux decline due to membrane fouling.

4. SEM images show that there is no membrane fouling evident on the surface of membranes used for microfiltration of the designed semi-synthetic MWF.

5. Cooling and lubricity tests show that results for the designed semi-synthetic MWF cannot be distinguished from those of a commercial semi-synthetic MWF, when tested on both a drilling testbed designed for MWF comparisons and a tapping torque machine.

REFERENCES

1. van Antwerpen, F., 2000, "Removal Fluids on the Move," Coolants/Lubricants for Metal Cutting & Grinding: Technology & Market Outlook 2000, Gorham Advanced Materials, Inc., Chicago, IL.

2. NIOSH, 1998, *Criteria for a Recommended Standard: Occupational Exposure to Metalworking Fluids*, National Institute of Occupational Safety and Health, Cincinnati, OH.

3. Marano, R. S., Cole, G. S., and Craudner, K. R., 1991, "Particulate in Cutting Fluids: Analysis and Implications in Machining Performance," Lubrication Engineering, **47**, pp. 376-382.

4. Abanto, M., Byers, J., and Noble, H., 1994, "The Effect of Tramp Oil on Biocide Performance in Standard Metalworking Fluids," Lubrication Engineering, **50**, pp. 732-737.

5. Skerlos, S. J., Rajagopalan, N., DeVor, R. E., Kapoor, S. G., and Angspatt, V. D., 2000, "Ingredient-Wise Study of Flux Characteristics in the Ceramic Membrane Filtration of Uncontaminated Synthetic Metalworking Fluids, Part 1: Experimental Investigation of Flux Decline," ASME Journal of Manufacturing Science and Engineering, **122**(4), pp. 739-745.

6. Skerlos, S. J., Rajagopalan, N., DeVor, R. E., Kapoor, S. G., and Angspatt, V. D., 2000, "Ingredient-Wise Study of Flux Characteristics in the Ceramic Membrane Filtration of Uncontaminated Synthetic Metalworking Fluids, Part 2: Analysis of Underlying Mechanisms," ASME Journal of Manufacturing Science and Engineering, **122**(4), pp. 746-752.

7. Mahdi, S. M., and Skold, R. O., 1990, "Field Testing of a Model Waterbased Metalworking Fluid Designed for Continuous Recycling Using Microfiltration," Lubrication Engineering, **47**, pp. 653-659.

8. Mahdi, S. M., and Skold, R. O., 1991, "Experimental Study of Membrane Filtration for the Recycling of Synthetic Waterbased Metalworking Fluids," Lubrication Engineering, **24**, pp. 389-395.

9. Rajagopalan, N., Boddu, V. M., Mishra, S., and Kraybill, D., 1998, "Pollution Prevention in an Aluminum Grinding Facility," Metal Finishing, **96**, pp. 18-24.

10. Skerlos, S. J., Rajagopalan, N., DeVor, R. E., Kapoor, S. G., and Angspatt, V. D., 2001, "Microfiltration of Polyoxyalkylene Metalworking Fluid Lubricant Additives Using Aluminum Oxide Membranes," ASME Journal of Manufacturing Science and Engineering, **123**(4), pp. 692-699.

11. Belfort, G., Davis, R. H., and Zydney, A. L., 1994, "The Behavior of Suspensions and Macromolecular Solutions in Cross-Flow Microfiltration," Journal of Membrane Science, **96**, pp. 1-58.

12. Glenn, T. F., and van Antwerpen, F., 1998, "Opportunities and Market Trends in Metalworking Fluids," Lubrication Engineering, August 1998, pp. 31-34.

13. Byers, J. P., ed., 1994, *Metalworking Fluids*, Marcel Dekker, New York, NY.

14. Rajagopalan, N., Rusk, T., and Dianovsky, M., 2004, "Purification of Semi-synthetic Metalworking Fluids by Microfiltration," Tribology & Lubrication Technology, **60**, pp. 38-44.

15. Rusk, T., and Rajagopalan, N., 2003, "Evaluation of Aged and Recycled Metalworking Fluids by the Tapping Torque," Lubrication Engineering, **59**, pp. 10-14.

16. Greeley, M. H., 2002, "Evaluations of Metalworking Fluid Functionality Using a Novel Drilling-Based Methodology," Masters Thesis, University of Illinois at Urbana-Champaign, Graduate College.

17. Mueller, J., Cen, Y., and Davis, R. H., 1997, "Crossflow Filtration of Oily Water," Journal of Membrane Science, **129**, pp. 221-235.

18. Tracey, E. M., and Davis, R. H., 1994, "Protein Fouling of Track-Etched Polycarbonate Microfiltration Membranes," Journal of Colloid and Interface Science, **167**, pp. 104-116.

19. Lee, S. B., Aurelle, Y., and Roques, H., 1984, "Concentration Polarization, Membrane Fouling and Cleaning in Ultrafiltration of Soluble Oil," Journal of Membrane Science, **19**, pp. 23-28.

20. Park, S. H., Yamaguchi, T., and Nakao, S., 2001, "Transport Mechanism of Deformable Droplets in Microfiltration of Emulsions," Chemical Engineering Science, **56**, pp. 3539-3548.

21. Hilal, N., Ogunbiyi, O. O., Miles, N. J., and Nigmatullin, R., 2005, "Methods Employed for Control of Fouling in MF and UF Membranes: A Comprehensive Review," Separation Science and Technology, **40**, 1957-2005.

22. Ma, H. M., Bowman, C. N., and Davis, R. H., 2000, "Membrane Fouling Reduction by Backpulsing and Surface Modification," Journal of Membrane Science, **173**(2), pp. 191-200.

23. Ezzati, A., Gorouhi, E., and Mohammdi, T., 2005, "Separation of Water in Oil Emulsions Using Microfiltration," Desalination, **185**, pp. 371-382.

24. Wentz, J. E., Kapoor, S. G., DeVor, R. E., and Rajagopalan, N., 2005, "Experimental Investigation of Membrane Fouling Due to Microfiltration of Semi-Synthetic Metalworking Fluids," Transactions of NAMRI/SME, **33**, pp. 281-288.

25. Zhao, F., 2005, "Microfiltration Recycling of Semi-Synthetic Metalworking Fluids: Modeling and Formulation Design," Ph.D. Thesis, University of Michigan.

26. Zhao, F., Urbance, M., and Skerlos, S., 2004, "Mechanistic Model of Coaxial Microfiltration for Semi-synthetic Metalworking Fluid Microemulsions," ASME Journal of Manufacturing Science and Engineering, **126**(3), pp. 435-444.

27. Nunn, C. C., 1981, "Equilibrium Adsorption onto Alumina from Some Solubilized Systems," Ph.D. Thesis, University of Texas at Austin.

28. Hirva, P. and Pakkanen, T. A., 1992, "The Interaction of Amine Bases on the Lewis Acid Sites of Aluminum Oxide – a Theoretical Study," Surface Science, **277**, pp. 389-394.

29. Kasprzyk-Hordern, B., 2004, "Chemistry of Alumina, Reactions in Aqueous Solution and its Application in Water Treatment," Advances in Colloid and Interface Science, **110**, pp. 19-48.

30. Verewey, E. J. W., and Overbeek, J. T. G., 1948, *Theory of Stability of Lyophobic Colloids*, Elsevier, Amsterdam.

31. Silliman, J. D., 1992, *Cutting and Grinding Fluids: Selection and Application*, SME, Dearborn, MI.

32. Johnson, T. L., 1990, "A Novel Oxazoline Compound for use in Metalworking Fluid Formulations," Lubrication Engineering, May 1990, pp. 279-284.

33. Ramachandran, V., Venkatesan, R., Tryggvason, G., and Fogler, H. S., 2000, "Low Reynolds Number Interactions Between Colloidal Particles Near the Entrance to a Cylindrical Pore," Journal of Colloid and Interface Science, **229**, pp. 311-322.

APPENDIX A – CLEANING RESULTS

Table A.1 - Result of Dawn Surfactant Cleanings

MWF Concentration	Run #	CWF (LMH) Before	CWF (LMH) After	Efficiency
1%	1	618	682	0.18
1%	2	513	649	0.29
1%	3	420	595	0.31
1%	4	391	581	0.32
3%	1	498	767	0.56
3%	2	545	719	0.40
3%	3	625	682	0.16
3%	4	515	643	0.28
5%	1	433	634	0.37
5%	2	426	645	0.40
5%	3	412	631	0.39
5%	4	440	690	0.46
Original CWF = 979 LMH				

Table A.2 – Result of Membrane Cleanings Using Other Surfactants

MWF Concentration	Cleaning Agent	CWF (LMH) Before	CWF (LMH) After	Change (LMH)	Efficiency
5%	2% Dawn Dish Detergent	200	274	74	0.280
5%	2% Simple Green Cleaner	274	277	3	0.283
5%	2% Tide Laundry Detergent	277	345	68	0.352
5%	Bake at 800C	345	979	634	1.000

Table A.3 – Result of Pyrolysis Cleaning

Cleaning #	Temp	CWF (LMH) Before	CWF (LMH) After	Efficiency
1	800	277	979	1.00
2	800	391	940	0.93
3	800	594	986	1.02
4	800	440	901	0.86
Original CWF = 979 LMH				

APPENDIX B – MEMBRANE SEM IMAGES

B.1 New Membranes
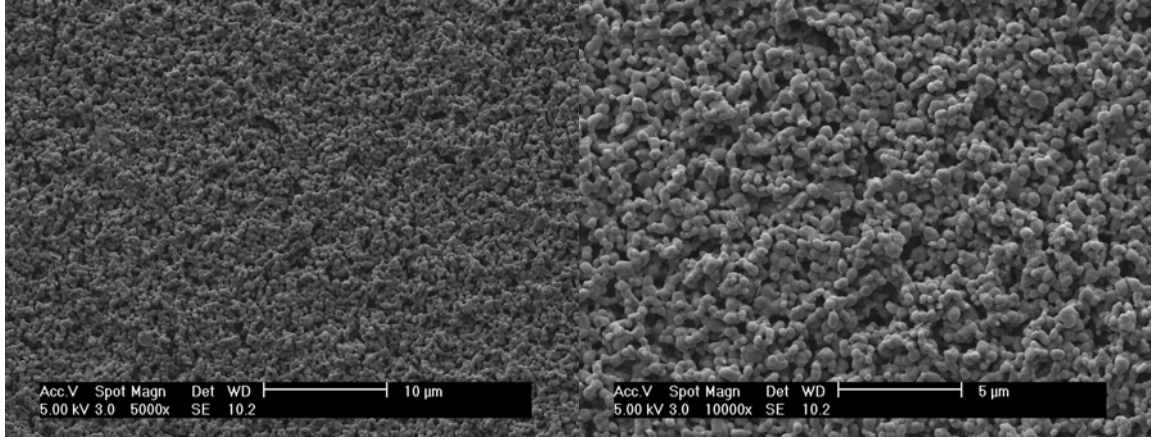
Figure B.1 – New Membrane Under 5000x and 10000x Magnification
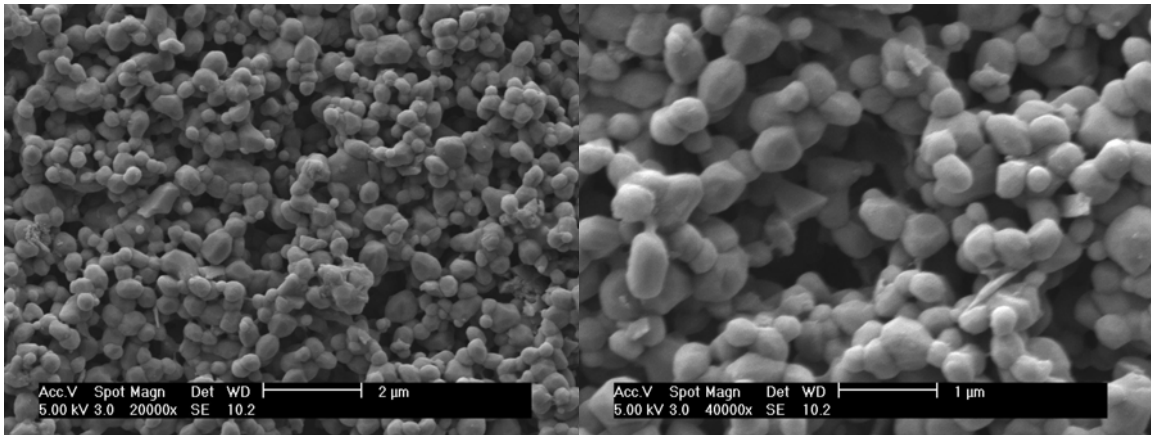
Figure B.2 – New Membrane Under 20000x and 40000x Magnification

B.2 Stage "A" Membrane Fouling
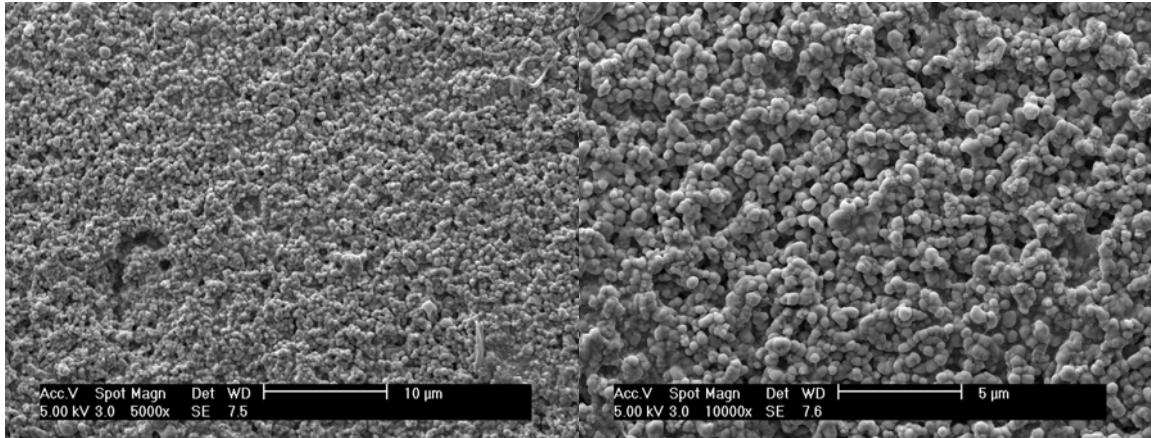
Figure B.3 – Stage "A" Membrane Fouling at 5000x and 10000x Magnification
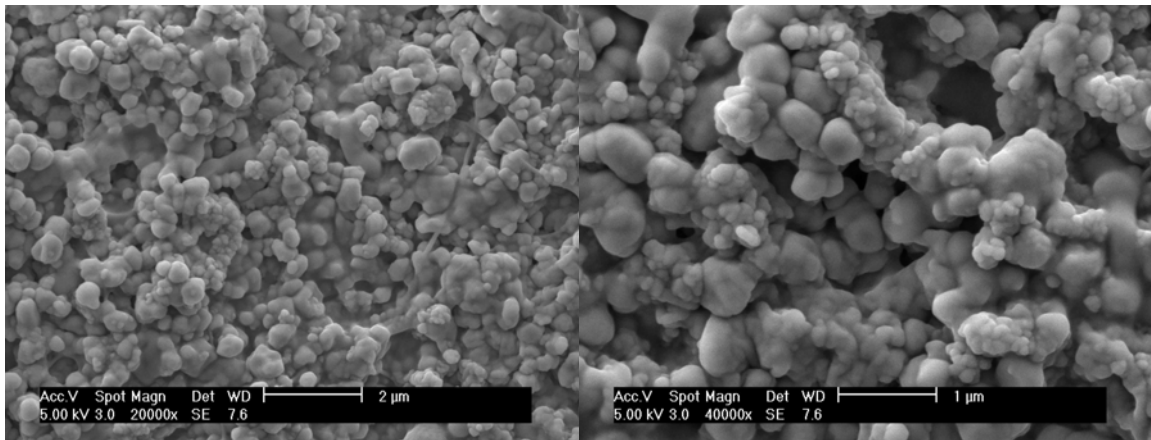
Figure B.4 – Stage "A" Membrane Fouling at 20000x and 40000x Magnification
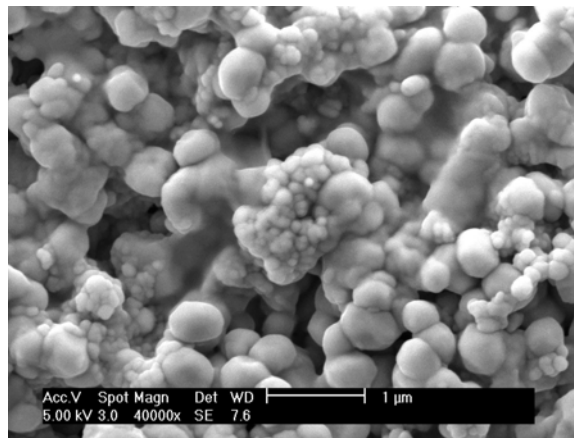
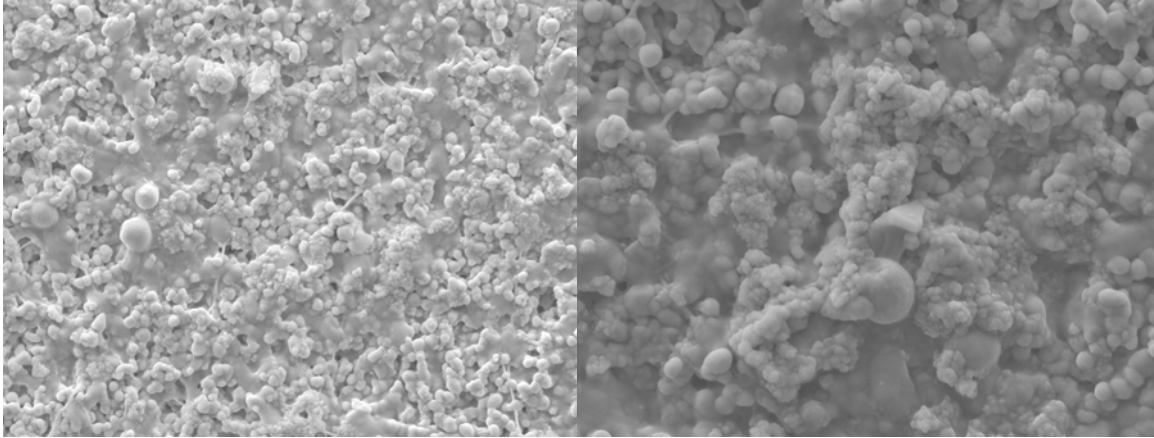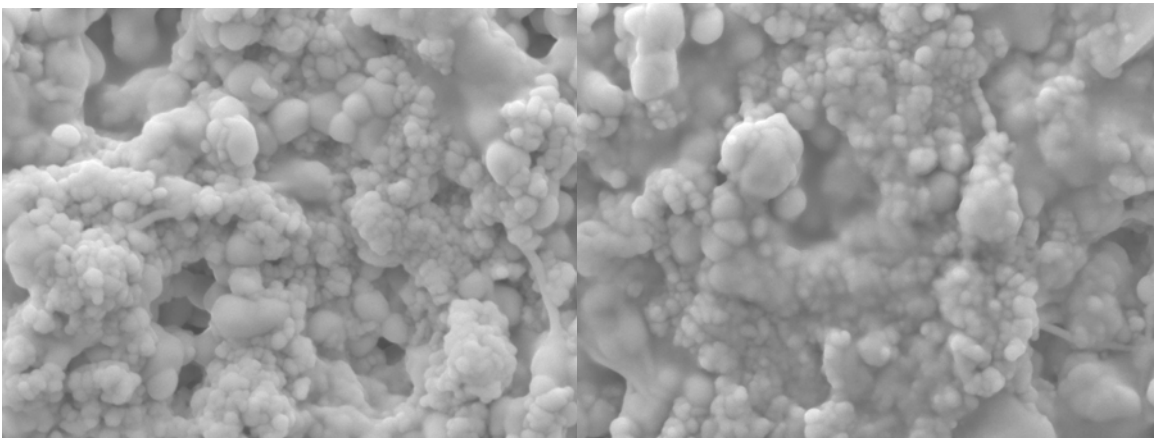Figure B.5 - Stage "A" Membrane Fouling at 40000x Magnification

B.3 Stage "B" Membrane Fouling

Figure B.6 – Stage "B" Membrane Fouling at 10000x and 20000x Magnification
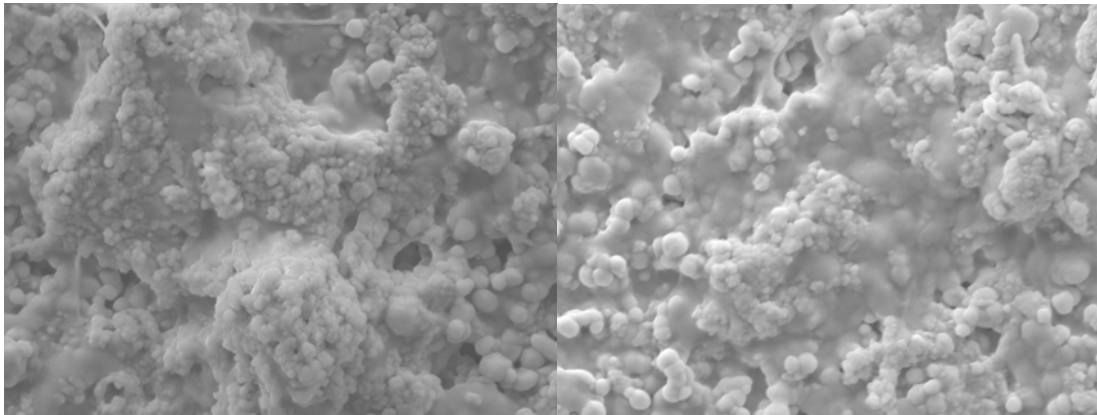
Figure B.7 - Stage "B" Membrane Fouling at 20000x Magnification

Figure B.8 - Stage "B" Membrane Fouling at 40000x Magnification

B.3 Membranes Following Surfactant Washing
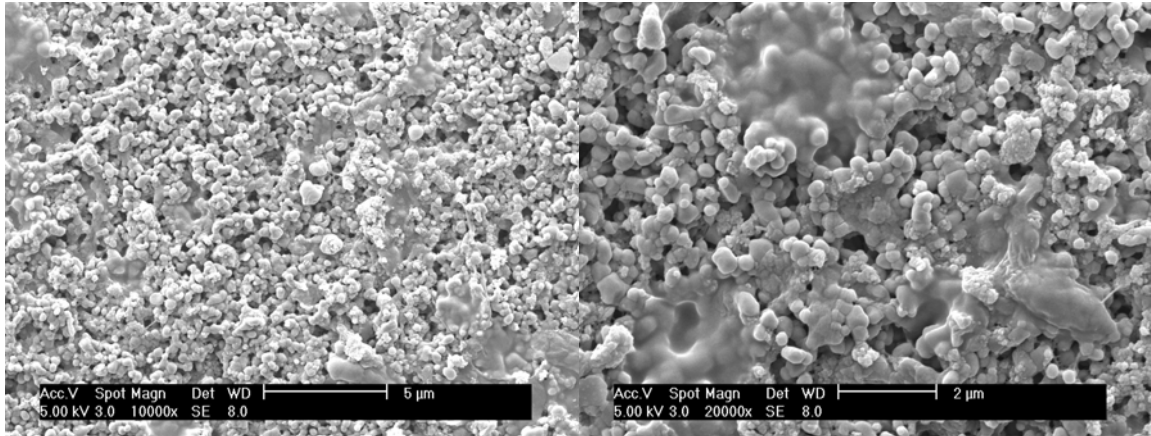
Figure B.9 – Surfactant Washed Membranes at 10000x and 20000x Magnification
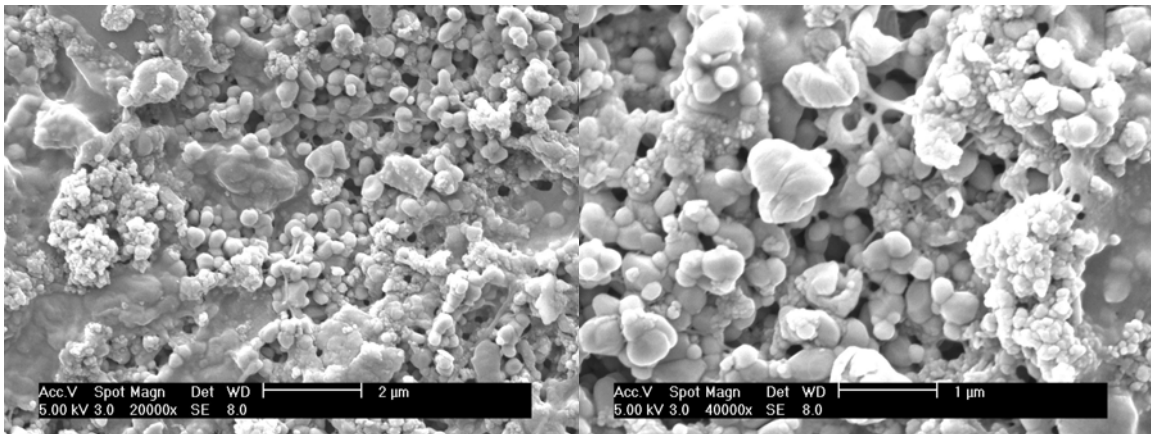
Figure B.10 – Surfactant Washed Membranes at 20000x and 40000x Magnification

B.4 Membranes statically exposed to MWF with no cross-flow.
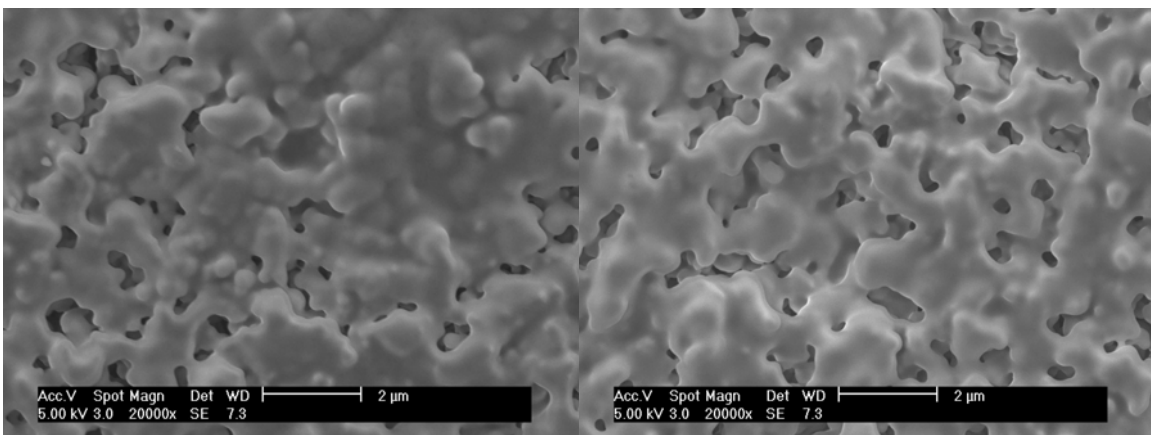
Figure B.11 – Membranes statically exposed to commercial MWF at 20000X Magnification

B.5 Membranes Introduced to MWF Components from Section 4
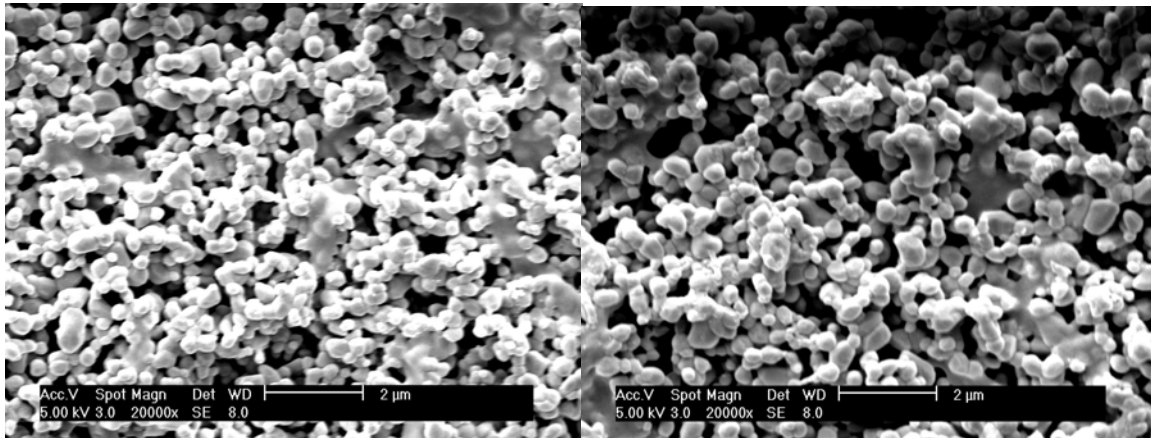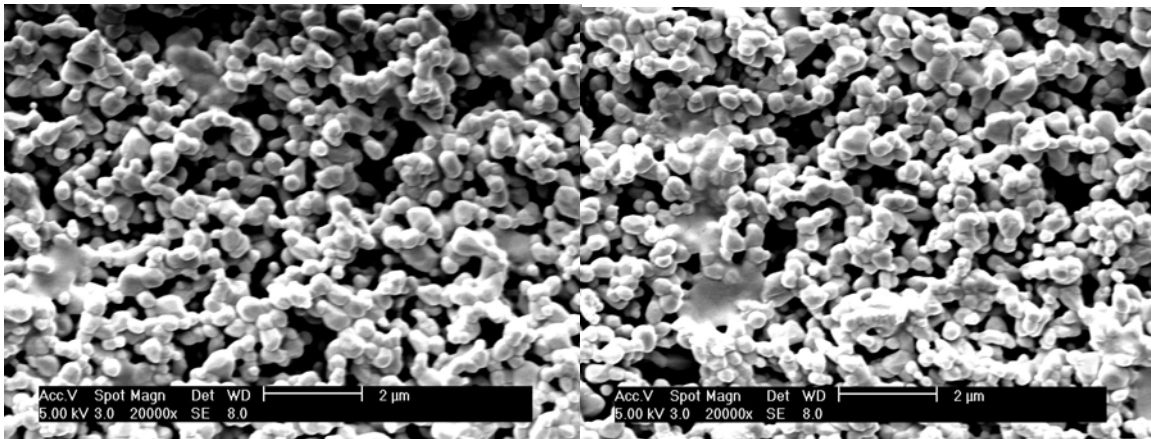

Figure B.12 – Control Membrane at 20000x Magnification

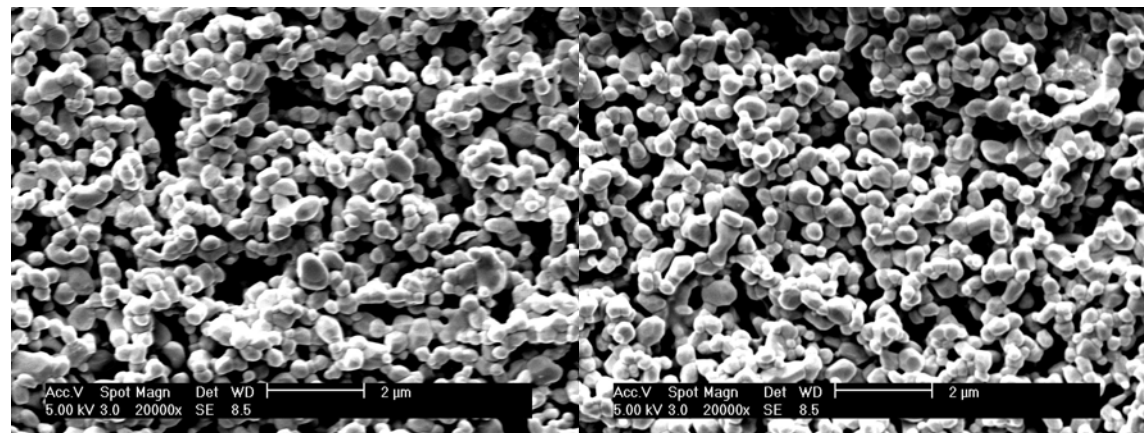Figure B.13 –Fluid 1 and Fluid 2 Membranes at 20000x Magnification

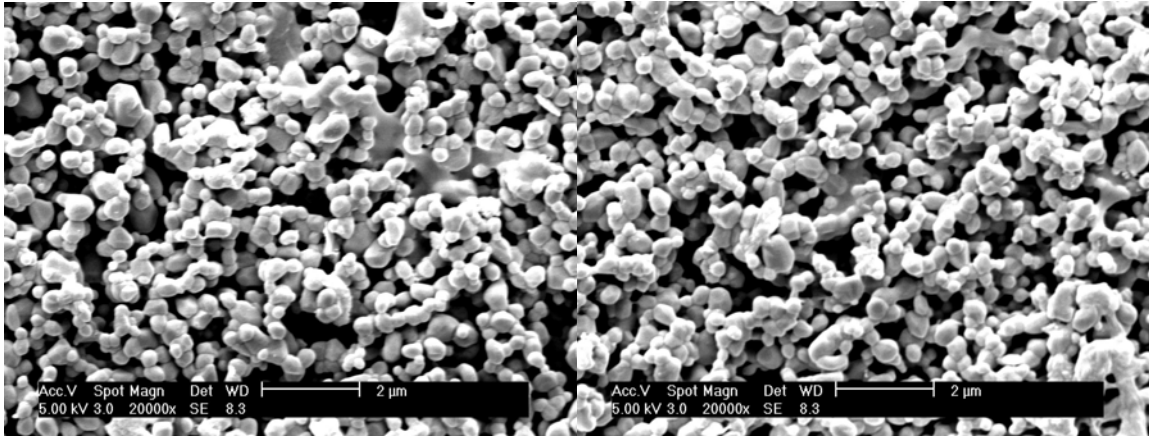Figure B.14 –Fluid 3 and Fluid 4 Membranes at 20000x Magnification

Figure B.15 –Fluid 5 and Fluid 6 Membranes at 20000x Magnification

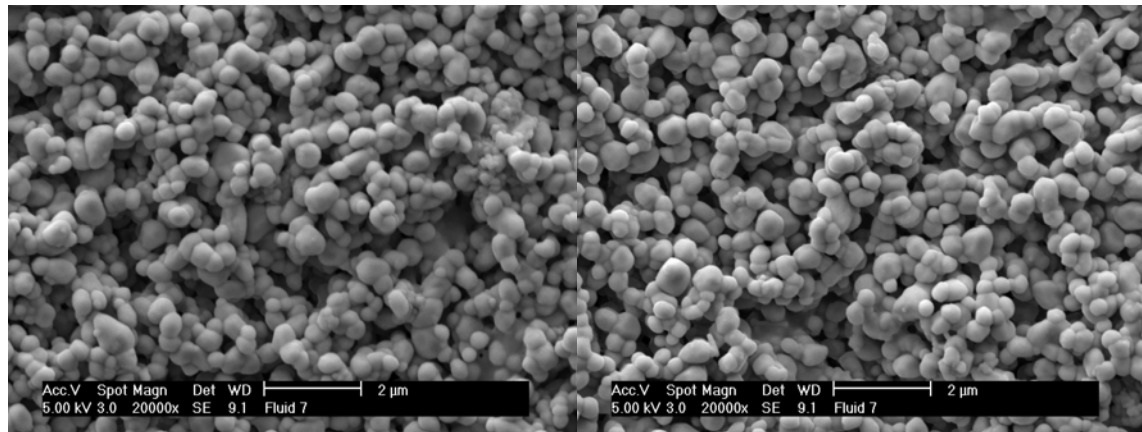**B.6 Membranes Used with Designed Fluid from Section 4**

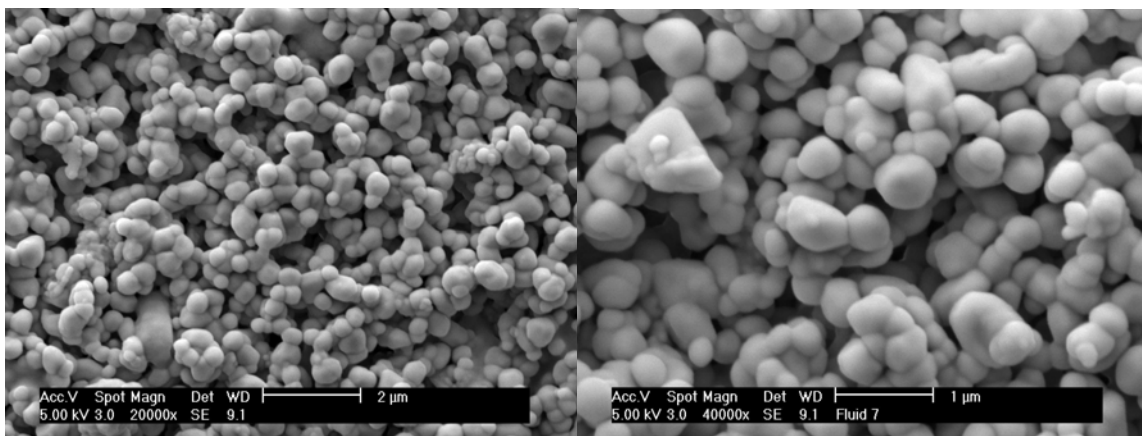Figure B.16 – Membranes Used with Fluid 6 at 20000x Magnification

Figure B.17 – Membranes Used with Fluid 6 at 20000x and 40000x Magnification

APPENDIX C – PUBLICATIONS

Two peer-reviewed publications were written stemming from the research provided

within this report. The first publication "Experimental Investigation of Membrane

Fouling Due to Microfiltration of Semi-Synthetic Metalworking Fluids" was published in

2005 in the Transactions of NAMRI/SME, Vol. 33, pp.281-288. It was also presented at

the 33rd Annual North American Manufacturing Research Conference, May 24-27, 2005

in New York, NY. The abstract for this publication is available at:

http://www.sme.org/cgi-bin/get-item.pl?TP05PUB179&2&SME&.

The second publication "Development of a Novel Metalworking Fluid Engineered for use

with Microfiltration Recycling" was published in January 2007 in the ASME Journal of

Tribology, Vol. 129, pp. 135-142. The abstract for this article is available at:

http://dx.doi.org/10.1115/1.2401207.